Sediment Erosion on Pelton Turbines: A Review

Xinfeng Ge[1]*, Jie Sun[1], Dongdong Chu[2], Juan Liu[3], Ye Zhou[3], Hui Zhang[4], Lei Zhang[5], Huixiang Chen[1], Kan Kan[1], Maxime Binama[1] and Yuan Zheng[1]

Abstract

The Pelton turbine has been widely used to develop high-head water resources with sediments because of its advantages in life cycle costs. When a flood or monsoon season occurs, the sediment concentration in the river increases suddenly, causing severe erosion to the nozzle, needle, and runner of Pelton turbines. After decades of development, researchers have developed practical engineering experience to reduce the sediment concentration of the flow through the turbine and ensure the safety and efficiency of power generation. Research on the mechanism of sediment erosion, development of anti-erosion materials, and establishment of erosion prediction models have attracted scholarly interest in recent years. Extensive research has been conducted to determine a complete and valuable syndication erosion model. However, owing to the complexity of the flow and wear mechanisms, the influence of specific parameters of erosion and the syndication effect is still difficult to determine. Computational fluid dynamics and erosion monitoring technology have also been evaluated and applied. This paper presents a comprehensive review of the erosion of Pelton turbines, some of the latest technical methods, and possible future development directions.

Keywords Pelton turbine, Sediment erosion, Sediment erosion mechanism, CFD, The experimental method

1 Introduction

Hydropower plays a key role in today's world as a vital renewable energy source. Hydropower accounts for the largest proportion of renewable energy. By 2018, the global installed capacity of hydropower had reached 1292 GW [1]. As the world's largest hydropower producer, China has an installed capacity of 352.3 GW [2]. However, several rivers worldwide have high sediment concentrations. For example, in 2019, the Yellow River, which has the largest sediment load, had an annual sediment discharge of 168 million tons [3]. The river sediment concentrations in the Himalayas, Andes, Alps, Pacific coastal mountains, and Nepal are among the world's largest. With global warming, melting glaciers, and frequent rainstorms, turbines installed in these river areas suffer from severe sediment abrasion [4–10]. Power interruption and maintenance caused by sediment problems disrupt the economic benefits of power stations. Sediment abrasion, cavitation, and corrosion combine to cause more damage to metallic materials. In addition, silt erosion aggravates vibration and fatigue damage, shortens a unit's life, increases maintenance costs, and threatens the safety and stable operation of the unit. All these factors adversely affect national electricity consumption [11–15].

For all hydropower stations installed on a high silt river, the eroded parts and erosion rates differ according to the various heads. Generally, power plants with medium and high heads are eroded more severely [16, 17]. The installed head of Francis turbines is often 30–700 m, and

*Correspondence:
Xinfeng Ge
gexinfeng@hhu.edu.cn
[1] College of Energy and Electrical Engineering, Hohai University, Nanjing 210098, China
[2] Jiangsu Water Conservancy Research Institute, Yangzhou 210017, China
[3] Institute for Hydraulic Machinery, China Institute of Water Resources and Hydropower Research, Beijing 100038, China
[4] Chongqing Shipping Construction Development Co., Ltd., Chongqing 500000, China
[5] Yellow River Institute of Hydraulic Research, Zhengzhou 450003, China

Ge *et al. Chinese Journal of Mechanical Engineering*   (2023) 36:64

Page 2 of 27

the runner, guide vanes, bottom ring, and labyrinth ring are easily eroded [18, 19]. The installed head of Pelton turbines is often 30–3000 m, and nozzles, needles, and buckets are easily eroded [20]. A large part of the head sections of the Pelton and Francis turbines coincide, as shown in Figure 1. However, the Pelton turbine has more advantages in terms of life cycle cost, has a head of 300–2000 m, and eroded parts are easier to replace [21, 22]. Therefore, Pelton turbines are widely used in high-head and sediment basins.

Impulse turbines include Pelton, Turgo, and cross-flow turbines. Among these, the Pelton turbine is the most efficient and widely used [24]. The Pelton turbine was invented in 1880 [25], and its performance was significantly improved [26] after experimental tests [27] and optimizations [28–37]. The characteristic of the Pelton turbine is that the centerline of the working jet is tangent to the runner's pitch circle. The main components are an inlet pipe, injector, runner, regulating mechanism, and casing. The inlet pipe distributes the water evenly to the injector, which converts the pressure energy into kinetic energy. The high-speed jet periodically impacts each bucket of the runner to complete the conversion of kinetic energy into

mechanical energy, and the flow rate and output torque can be adjusted through the movement of the needle. The most common arrangement of a Pelton turbine is shown in Figure 2. The Turgo turbine was invented in 1920 [38], and its applied head is 15–300 m. Because of the lower application of Turgo and cross-flow turbines, this paper focuses on introducing the Pelton turbine.

Pelton turbines are susceptible to erosion by sediment-laden flows, and the basic mechanisms of sediment erosion are cutting, fatigue, and brittle failure of materials [20]. The efficiency of the turbine is affected by erosion, as shown in Figure 3. This is the curve between the width of the splitter and the decrease in efficiency [41]. Three main factors affect the sediment erosion:

a. Factors related to the operating conditions, such as flow rate, velocity, impact angle, temperature, and fluid medium.
b. Factors related to the physical parameters of sediment, such as particle size, concentration, shape, and density.
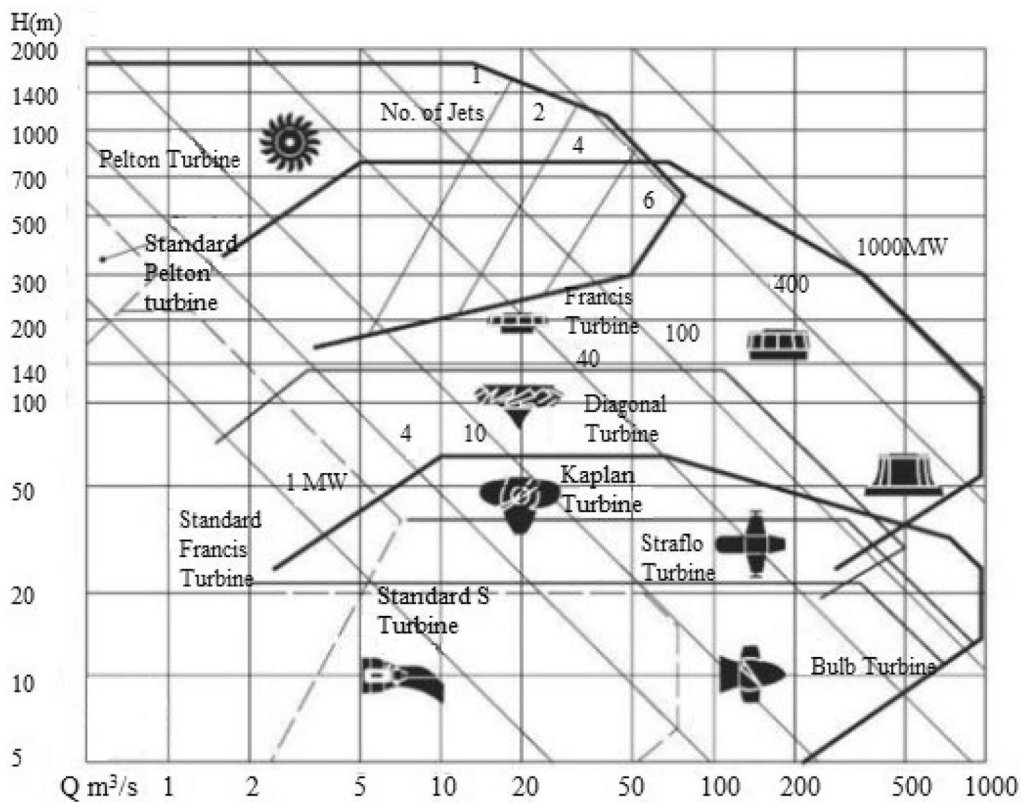c. Properties of flow-passage components, such as chemical properties, materials, and coatings.

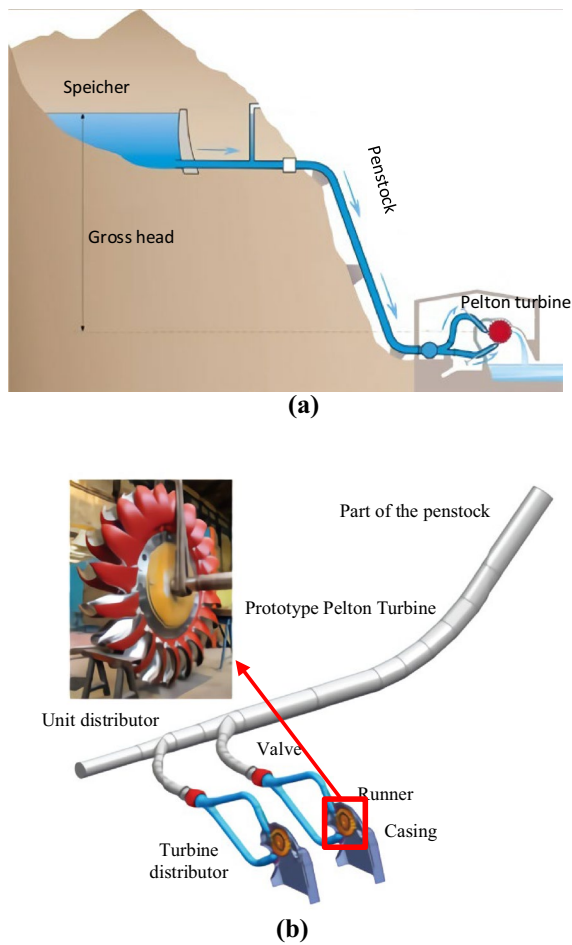**Figure 1** Turbine application chart [23]

Ge *et al. Chinese Journal of Mechanical Engineering*   (2023) 36:64

Page 3 of 27

(a)

(b)

Figure 2 Typical layouts of the Pelton turbine [39, 40]
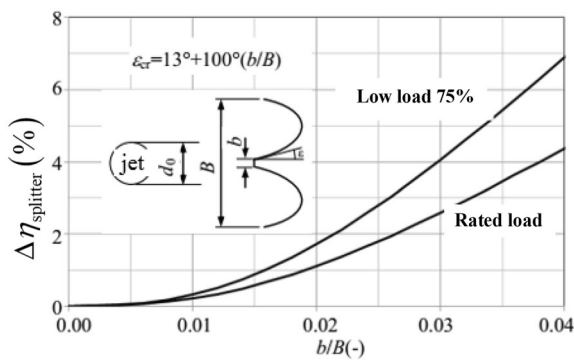

Figure 3 Calculated efficiency drops caused by eroding main splitters of Pelton buckets [41]

The surface of the damaged metal is characterized by fish-scale pits, ripples, and grooves. Sediment erosion is often combined with cavitation and chemical corrosion, resulting in the large-area spalling of the material [42].

The methods generally used to study Pelton turbines are field cases, experiments, and computational fluid dynamics (CFD). From the initial stage of operation of the Pelton power station, it has encountered a severe problem of sediment erosion. To solve practical problems, engineers have proposed many methods, such as building sand traps, replacing runner materials, and stopping operations during high sediment periods [11, 17, 43]. Researchers have systematically studied sediment erosion from both experimental and theoretical perspectives [5, 6, 44–46]. In the 20th century, CFD was significantly developed, and the first numerical simulation study on the Pelton turbine appeared in 1998 [47]. Currently, researchers can use CFD to study the unsteady complex flow phenomenon more deeply, promoting the sediment erosion problem and dramatically improving runner performance [16].

In addition to the methods mentioned above, theoretical research, erosion monitoring technology, and standard protective measures have been developed. The aim of this paper is to provide a comprehensive overview of the erosion of Pelton turbines, some of the latest technical methods, and possible future development directions.

2 Field Case Investigation

Many Pelton turbines installed in areas with high sediment-laden flow have suffered from severe erosion. An investigation of power stations indicated the following.

After an operation of 600 h with a net head of 920 m, the needle was severely eroded at a hydropower station in the Himalayas [15]. The injector of the Chennai power station was also severely eroded after 2712 h of operation [49]. The Khimki power station had been operating for only a year, and the splitter was eroded and serrated [7, 20]. For the Chilime power station with a capacity of 22 MW, the unit efficiency was reduced by 1.2% owing to sediment abrasion. The erosion rate of the bucket and needle was estimated to be 3.4 mm/year [50]. Technical experts suggested increasing the water level to solve sediment abrasion in the Kulekhani-I hydropower station with a 550 m head. Although the high sediment concentration was solved, the water storage and power generation capacity decreased [51]. The Zhala hydropower station in Tibet, with a total installed capacity of 1000 MW, has a head of 690.55 m and an average annual sediment concentration of 0.259 kg/m^3. The annual erosion depth of the bucket was estimated to reach 0.1 mm [52]. Two Pelton turbines installed in a power station in China were severely damaged after 1020 h of operation [53]. After the sediment period, the unit efficiency loss of the Fieschertal Power Station reached 1%. The depth of the cutout increased by 9 mm and the height of the splitter decreased by 6 mm [54]. The Alfalfal Hydropower

Station, with a head of 690 m, suffered severe erosion during its operation because of an uncoated runner. After technical improvements, two coatings were successively used: sxhtm70 and sxhtm8x. Even if the runner is coated, it is difficult to operate in a high-flood season without severe erosion [10].

Based on the above investigation, the conclusions are presented in Table 1. Figures 4 and 5 show examples of the eroded needle and runners in hydropower plants (HPPs). We can observe that the needle, splitter, and cutout are the most vulnerable parts of Pelton turbines.

The sediment particle size has different erosion tendencies for the needle and runner. Thapa and Brekke [57] observed that fine particles cause more severe erosion on the needle, coarse particles cause more severe erosion on the bucket, and medium-sized particles cause significant abrasion on the needle and bucket.

The erosion of the injector affects the quality of the jet and the energy transfer between the jet and runner. In particular, the eccentric jet may be caused by erosion, which causes the efficiency of the unit to decrease rapidly [58–61].

As an energy-conversion component, runner wear affects the output characteristics of the unit, resulting in a decrease in the torque. Therefore, the pattern and division of the runner erosion zone have also been the focus of research. Refs. [17, 41, 62–64] observed runner erosion at different power stations and divided the erosion zone of buckets into five parts (Figure 6). Although the erosion zone division of buckets is based on many cases, erosion position standards have not been widely promoted. However, this has not been applied in actual field evaluations.

Although the position of erosion and estimated erosion rate for maintenance can be measured by a case investigation, different HPPs have different conditions, and generalizing the empirical erosion formula is difficult.
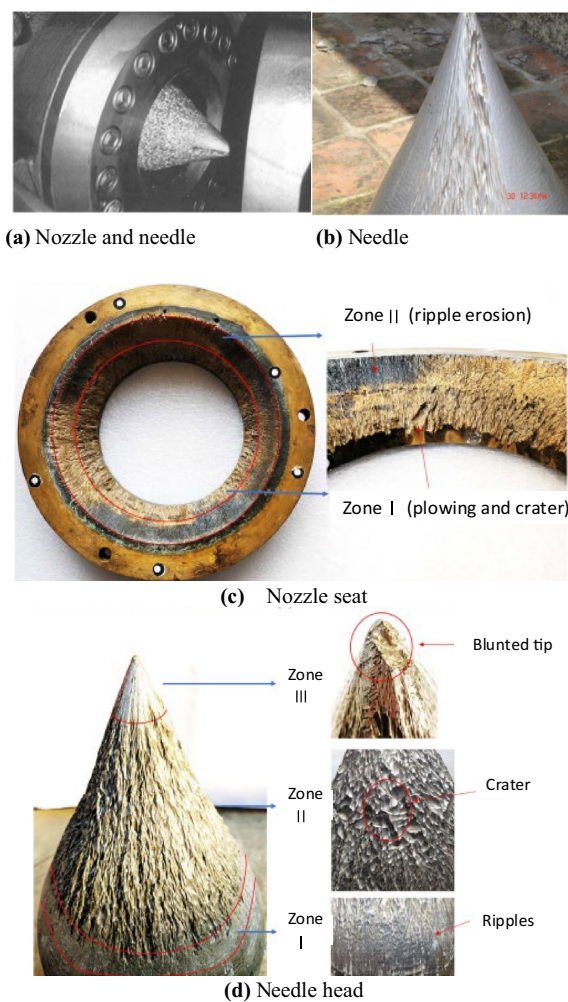

(a) Nozzle and needle   **(b)** Needle

(c) Nozzle seat

(d) Needle head

Figure 4 Field erosion of a needle [15, 49, 50]

Erosion assessment requires a large workforce and financial resources, but the results are not universal, which is very uneconomical for HPPs.

Table 1 Field case investigation

	Hydropower station	Head (m)	Capacity (MW)	Erosion phenomenon
1	Chilime HPP [50]	351.5	2×11	An efficient reduction of 1.21%; Wear rate of 3.4 mm/year was estimated for the needle and the bucket
2	Ref. [15]	920	–	The needle was seriously eroded
3	Chennai HPP [49]	365	5×4.66	The erosion was found to be 3.71% and 5% on spear and nozzle, respectively
4	Zhalia HPP [52]	690.55	4×250	The annual erosion depth of the bucket can reach 0.1 mm
5	Fieschertal HPP [54]	515	2×32	The depth of the cutout was increased by 9 mm, and the height of the splitter was reduced by 6 mm
6	Alfalfa HPP [10]	690	–	Coating with SXHTM70 decreased the damages significantly
7	Ref. [15]	645	81	The splitter's thickness increased to 1% of the bucket with the efficiency dropping to 1% at full load.
8	Toss HPP [8, 55]	174	2×5	The runner was seriously eroded
9	Jhimruk HPP [56]	205	12	Drop in the efficiency of 4% of the turbine unit

Figure 5 Field erosion of runners in different power stations: (a) Toss HPP, India [8]; (b) Alfalfal HPP, Chile [10]
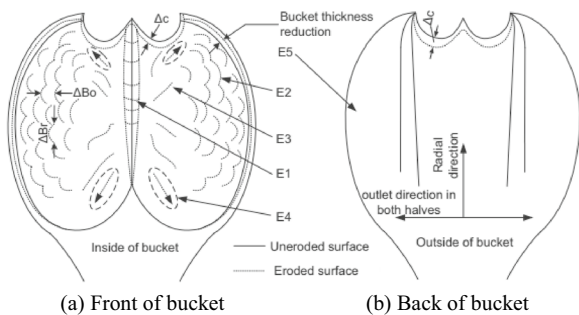

Figure 7 Rotating disc test system [44]

(a) Front of bucket   (b) Back of bucket

Figure 6 Classifications of the erosion position of buckets [62]

Figure 8 Runner fabricated from brass [6]

Researchers have used experimental methods to study Pelton turbines to determine erosion factors and an erosion model (Section 3).

3 Experimental Studies

Many sediment erosion test rigs exist, such as jet test benches, rotating discs, slurry pot testers, model units, and single bucket fixed experimental devices [65–67]. The experimental systems described below have been commonly used to study silt erosion in recent years.

3.1 Rotating Disk Test System

The rotating disk test system is a common experimental device used to study the multiphase-flow impact damage of hydraulic turbines. It was initially used to study sediment erosion of low-head turbines [68]. As shown in Figure 7, the high-head hydraulic mechanical erosion test system (ETS-HM) was developed by the China Institute of Water Resources and Hydropower (IWHR). The experimental device comprises a rotating disc, nozzle, and erosion chamber. During an experiment, a trapezoidal specimen is fixed to a support plate. The motor controls the disc speed, and the high-speed jet is ejected from the nozzle. Liu et al. [44, 69, 70] used this device to test the anti-erosion properties of different materials with different sediment characteristics (concentration, hardness, and mineral content). Erosion prediction models for different materials were established based on
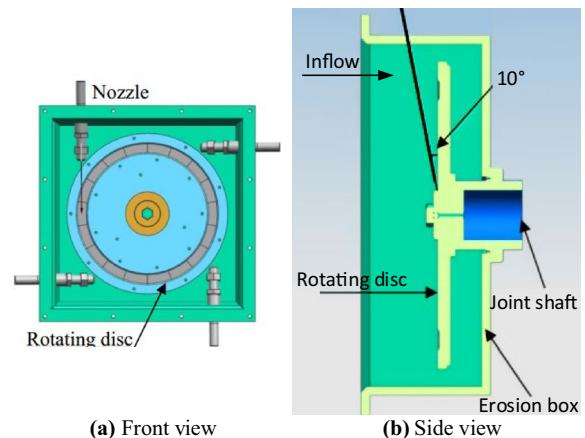
experimental data and multiple linear regression analyses. Subsequently, the erosion rates of the Pelton turbine flow passage components in the Tibet and Pakistan Allai Khwar power stations were evaluated.

3.2 Pelton Turbine Test Rig

Because the actual flow process is complex, it is impossible to consider the changes in the bucket surface curve and jet angle on the rotating disc. Therefore, more scholars have used the Pelton turbine model unit to conduct experiments.

Padhy et al. [5] collected sediment from the Bhagirathi River. After screening and drying, it was added to a water tank and stirred evenly to simulate sediment-laden flow under natural conditions. Subsequently, an experiment was conducted on a small Pelton turbine. The runner fabricated from brass is shown in Figure 8. By weighing the runner after the test, the related data of sediment parameters and runner mass loss under different velocities, particle sizes, and concentrations were collected, and the first-order regression expression of the erosion rate was established. Later, based on this test, these scholars further studied the relationship between efficiency loss and erosion parameters and obtained a correlation expression

Ge *et al. Chinese Journal of Mechanical Engineering*   (2023) 36:64

Page 6 of 27

and error range of ±10% [6]. Thakur et al. [71] also studied the factors influencing bucket erosion using similar devices and research methods. The device is shown in Figure 9, and the error between the erosion model and experimental data was within ± 12.8%.

3.3 Pelton Turbine Rig for Hydro-Abrasive Erosion Testing

Although the Pelton turbine model unit in Section 3.2 is closer to the actual operating conditions than the rotating disc, because experimental results should be obtained quickly, the materials used are metals with low hardness, such as brass. The difference in materials results in

Figure 9 Experimental devices of a small Pelton turbine [71]

different wear results for an actual turbine. Rai et al. [48] summarized and analyzed the advantages and disadvantages of previous experimental devices and proposed a new device, as shown in Figure 10. Rai et al. [72] not only verified the accuracy of the test rig but also proposed using an optical scanner and weighing method to simultaneously measure the bucket erosion and mass loss to ensure the accuracy of the measurement [48]. Rai et al. [45] conducted erosion experiments on runners of different materials to compensate for defects in which the runner material is brass. They summarized the exponential constant values of the velocity, concentration, size, and time.

3.4 Summary

According to references, in the experimental process, the more consistent the test conditions with the field test conditions, the more accurate the results [73]. Jet test rigs focus on the abrasion resistance of materials [20, 74]. Simulating the actual erosion conditions of Pelton turbines using a slurry pot tester is challenging [48]. The limitations of a single bucket fixed experimental device are the lack of the Coriolis force, the Coanda effect, and secondary erosion [48]. For a rotating disk, the bucket shape and jet angle change cannot be considered. Although the Pelton turbine model unit is closer to field operating conditions, the material used differs significantly from the actual material. The Pelton turbine rig for hydro-abrasive erosion testing is closest to the field unit in terms of material and operating conditions. However, it has some limitations:
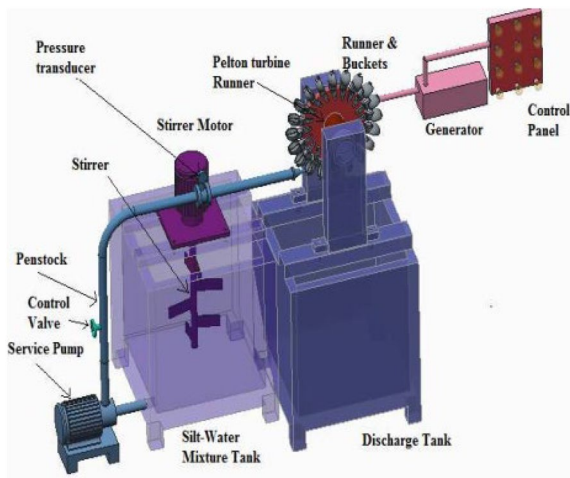
Figure 10 Diagram of Pelton turbine rig for hydro-abrasive erosion testing [72]

Ge *et al. Chinese Journal of Mechanical Engineering*   (2023) 36:64

Page 7 of 27

a. Observing sediment erosion, such as that during the monsoon season, often requires a long time. The experiment frequently requires several weeks; therefore, quantitatively observing the specific effect of certain sediment parameters is difficult.

b. Ensuring that the operating conditions of the prototype unit and experiment are entirely consistent is challenging.

Table 2 shows the erosion models developed by scholars according to experimental data. We can observe that under different experimental conditions, the test results differ significantly, and the influence of different parameters on the erosion results is not fully understood [48].

4 Theoretical Studies on Wear Mechanism

4.1 Research and Development of the Wear Mechanism of Sediment Particles

Scholars have discussed and analyzed the surface erosion patterns of hydraulic machinery [75]. The wear of hydraulic machinery is an action process involving a compound mechanism. The main reason for hydraulic machinery wear is sediment particle erosion. The wear mechanism is generally divided into impact and sliding wear [15], with impact wear playing a significant role in the wear mechanism. These two mechanisms are primarily caused by shear and deformation, as shown in Figure 11.

(a) Impact wear: A single particle impacts the solid surface at a certain speed and angle. After a long development period, the surface material undergoes microscale deformation, cutting, and fatigue cracks.

Table 2 Summary of erosion models based on experiments

Name	Time	Erosion models	Comments
Liu et al. [69]	2012	Needle tip (ZG230-450): $E = 5.45 \times 10^{-9} \cdot W^{3.16} \cdot C_s^{0.98}$ Needle shaft (42CrMo): $E = 1.47 \times 10^{-9} \cdot W^{3.41} \cdot C_s^{1.02}$ Runner bucket (X3CrNiMo13-4): $E = 8.82 \times 10^{-9} \cdot W^{3.51} \cdot C_s^{1.01}$	E is the erosion rate of mass loss for the test sample, g/h W is the resultant velocity, m/s C_s is the sediment concentration, kg/m^3
Liu et al. [44]	2019	Runner bucket (04Cr13Ni5Mo): $E = 3.45 \times 10^{-9} \cdot W^{4.31} \cdot C_s^{1.05}$ Needle tip (ADB610): $E = 5.32 \times 10^{-9} \cdot W^{4.28} \cdot C_s^{0.95}$ Nozzle ring (42ZG230-450): $E = 1.07 \times 10^{-8} \cdot W^{4.07} \cdot C_s^{1.06}$	E is erosion rate, μm/h W is the resultant velocity, m/s C_s is the sediment concentration, kg/m^3
Padhy et al. [5]	2009	Runner (brass): $W = 4.02 \times 10^{-12} S^{0.0567} C^{1.2267} V^{3.79} t$	W is normalized wear, g/g; per unit discharge, m^3/s S is silt particle size, m C is silt concentration, ppm V is silt concentration, m/s
Padhy et al. [6]	2011	Turbine (brass): $\eta\% = 2.43 \times 10^{-10} t^{0.75} S^{0.099} C^{0.93} V^{3.40}$	η is efficiency loss, % S is silt particle size, m C is silt concentration, ppm V is silt concentration, m/s
Thakur et al. [71]	2017	Runner blades (Aluminum): $W = 3.733 \times 10^{-11} S^{0.1159} C^{0.9096} V^{2.285} t^{1.1317}$	W is normalized wear, g/g S is silt size, μm C is the silt concentration, ppm V is the jet velocity, m/s t is operating time, h
Rai et al. [45]	2020	Bucket (Bronze): $(E_n)_{BGi} = 5.74 \times 10^{-12} (SSC)^{1.03} (d_{50})^{-0.085} (C)^{3.10} (t)^{1.09}$ Bucket (16Cr-5Ni): $(E_n)_{BGi} = 9.09 \times 10^{-13} (SSC)^{1.09} (d_{50})^{0.004} (C)^{3.36} (t)^{1.11}$ Bucket (16Cr-4Ni): $(E_n)_{BGi} = 7.02 \times 10^{-13} (SSC)^{1.08} (d_{50})^{-0.009} (C)^{3.42} (t)^{1.12}$ Bucket (13Cr-4Ni): $(E_n)_{BGi} = 6.25 \times 10^{-13} (SSC)^{1.08} (d_{50})^{0.000} (C)^{3.47} (t)^{1.11}$ Bucket (13Cr-4Ni with plasma sprayed Cr2O3 coating): $(E_n)_{BGi} = 7.14 \times 10^{-12} (SSC)^{1.25} (d_{50})^{0.376} (C)^{2.42} (t)^{1.18}$ Bucket (13Cr-4Ni with WC-Co-Cr HVOF coating): $(E_n)_{BGi} = 1.38 \times 10^{-14} (SSC)^{1.12} (d_{50})^{0.314} (C)^{4.09} (t)^{0.96}$	$(E_n)_{BGi}$ is normalized erosion for the bucket, g SSC is silt concentration, ppm d_{50} is median sediment size in a particle size distribution, mm C is relative flow velocity, m/s t is the time duration of erosion, h

Ge *et al. Chinese Journal of Mechanical Engineering*   (2023) 36:64

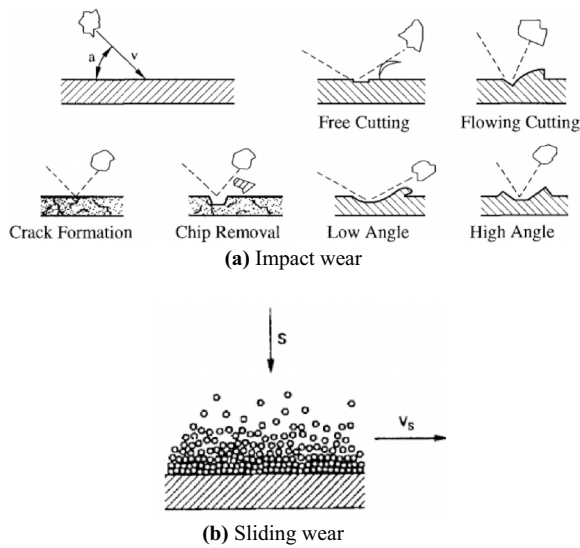Page 8 of 27

(a) Impact wear

(b) Sliding wear

Figure 11 Two wear mechanisms [15]

(b) Sliding wear: A large number of particles move along a solid surface at a tangential speed. After a long period of development, the scratching on the solid surface removes the material.

Sand erosion in hydraulic machinery can be divided into three types [15]:

a. Abrasive surface erosion caused by small particles with strong fluidity ($S \leq 60$ μm) at a high flow rate.
b. Vortex erosion of secondary flow at the bend of the channel.
c. The wear on the wall is caused by large particles ($S \geq 0.5$ mm) separated from the streamline.

After sand abrasion, according to the surface wear state of the metal materials, the wear can be classified as follows [15]: (a) metallic luster, (b) fine-scale erosion, (c) scaly erosion, (d) large-scale scaly erosion, (e) in-depth erosion, and (f) through holes or entire erosion out of the metal.

However, no quantitative model exists that describes the specific wear degree of a Pelton turbine. The expression of wear commonly used in the early days was as follows [76]:

$$Wear \propto (velocity)^n \tag{1}$$

where n is velocity index. Subsequently, many other wear models were developed [46, 50, 77–80]. In some authoritative studies and reference manuals, the wear models of the Pelton turbine are described as follows.

In the book "*Abrasive erosion and erosion of hydraulic machinery*", the following wear reference model is provided [15]:

$$J = \frac{A \cdot p \cdot t \cdot W^3}{\varepsilon}, \tag{2}$$

where J is the extent of the erosion (mm); p is the average annual concentration of abrasive particles (kg/m³); t is the time interval comprising the period within a year when abrasive particles attack the surface; W is the flow velocity (m/s); ε is the erosion resistance of the material used (equal to unity for carbon steel); A is the index of the slurry abrasively depending on the shapes of the particles and is to be determined experimentally (mm · s³/year).

The theoretical wear model proposed by the International Electrotechnical Commission (IEC) 62364 is as expressed follows [73]:

$$\frac{dS}{dt} = f(\text{particle velocity, concentration, physical properties,}$$

$$\text{flow pattern, turbine material properties, and other factors}), \tag{3}$$

where dS/dt is the hydroabrasive erosion rate (mm/year).

Although the IEC provides an empirical erosion model of hydraulic turbines, the model coefficient of the Pelton turbine is not provided because of the lack of field test data [62]. Based on the measured data of a power station, Rai et al. [8] supplemented and explained some parameters of the Pelton turbine in the IEC model, such as the flow coefficient (K_f), material factor (K_m), exponent (p), erosion depth (S), and shape factor (K_{shape}).

The erosion model has been developed for many years, but the current theoretical research lacks quantification of the erosion rate of each part of the Pelton turbine. Duan et al. [15] proposed that the erosion depth of a splitter can determine the erosion rate. Felix [81] proposed quantifying erosion by measuring the splitter's height change, cutout depth increase, and decrease in coating thickness. Rai et al. [8] also proposed a definition of the erosion depth for different parts to quantify erosion.

To study the mechanism of sediment erosion, in addition to analyzing the wear mechanism and establishing the corresponding wear formula, researchers use instruments such as stroboscopic photos and the scanning electron microscope (SEM) to verify these theories [82, 83]. Padhy et al. [83] verified the wear mechanism of particles using electron microscopy and studied the mechanism of the particle angle on bucket surface erosion. Using SEM, Rai et al. [46] observed that the erosion mechanisms of different bucket parts depended on the flow pattern.
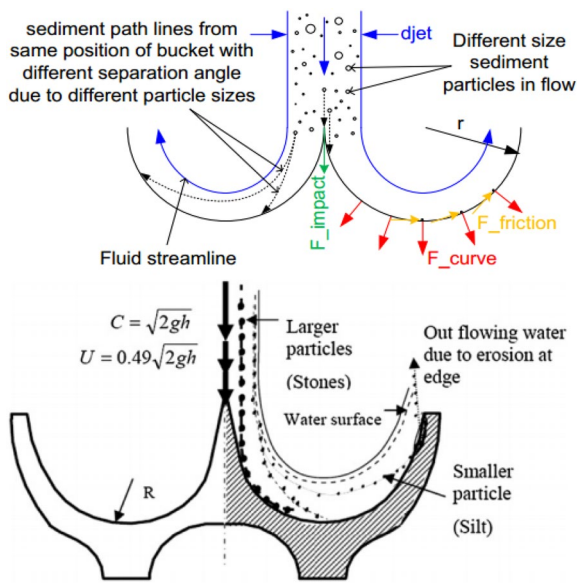
Ge *et al. Chinese Journal of Mechanical Engineering*   (2023) 36:64

Page 9 of 27

Figure 12 Effect of particle size on erosion position [20, 84]

In addition to the angle of particles, particle size significantly influences the erosion position and rate, as shown in Figure 12 [83, 84]. A high acceleration causes the particles to separate from the streamline, causing erosion of the material surface. Small particles are more likely to cause erosion at the outlet edge of the bucket, whereas large particles are more likely to cause erosion at the bucket inlet edge [83]. In addition, when the particles are

separated from the streamline, the local flow of the wake became turbulent. This turbulence produces unsteady loads and oscillations on particles, and may increase erosion [84].

Based on data collected from 250 power stations worldwide, Rai [84] analyzed the mechanism of sediment erosion of Pelton turbines from the perspective of mechanics. The forces acting on the runner during operation were divided into four types: (a) centrifugal force with constant magnitude and outward direction, (b) Coriolis force changing along the streamline, (c) constant force due to path curvature, and (d) drag. The forces in the bucket are shown in Figure 13.

Parray et al. [49] studied the erosion mechanism of an injector (Figure 14). In Zones I and II, the impact angle is relatively small, and the erosion pattern of the surface is primarily ripples caused by scratching. The impact of a large angle and high velocity in Zone III results in fatigue damage and fracturing of the needle tip.

4.2 Combined Effects of Sediment Erosion and Cavitation

Sand abrasive erosion, cavitation, corrosion, and casting defects of materials form a combined effect that aggravates erosion. However, the most important factor is the cavitation−abrasive erosion caused by the combined hydrodynamic force of cavitation and sediment particles. Cavitation erosion and sediment abrasion interact and influence each other [15]. The silt particles increase the concentration of the gas nucleus in the water, and the surface becomes rough after silt
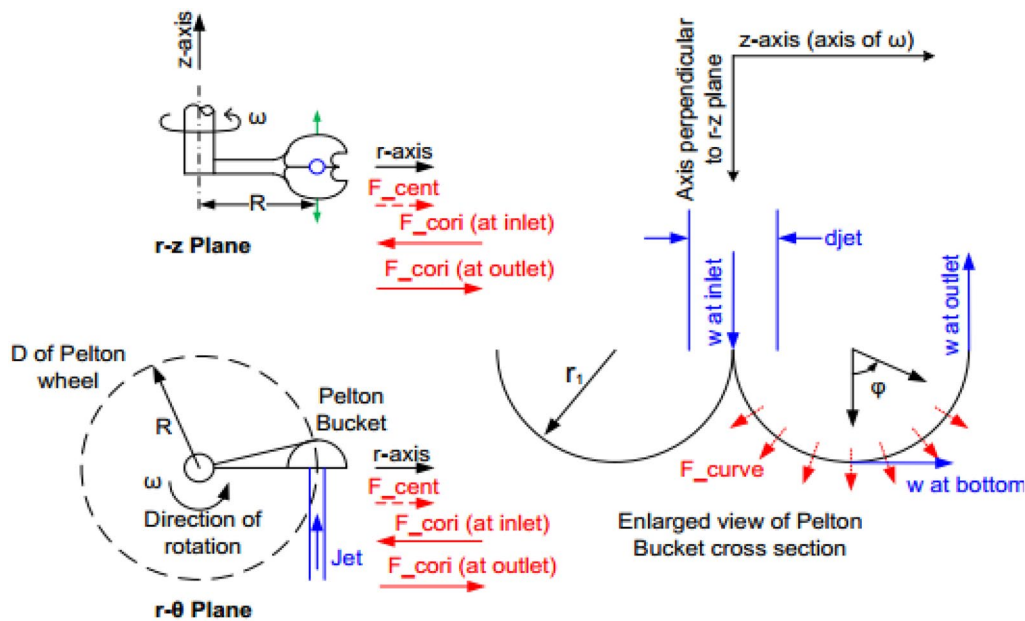

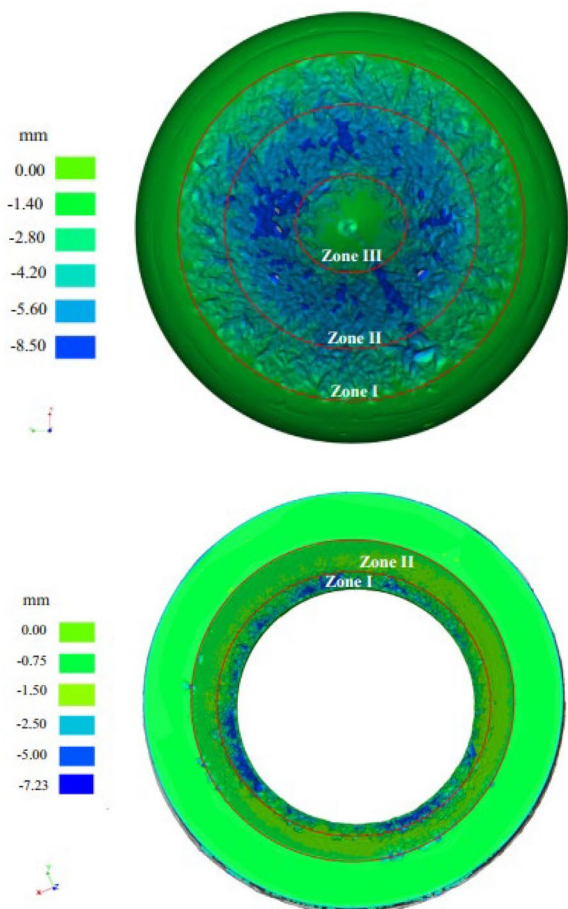**Figure 13** Simplified flow in the bucket and force direction [84]

Ge *et al. Chinese Journal of Mechanical Engineering*   (2023) 36:64

Page 10 of 27

Figure 14 Erosion zone of the nozzle and needle [49]

Figure 15 Comparison of the relative flow pattern inside the buckets between FVPM (left), VOF (middle), and experimental (right) for the impinging angles of 62°, 72°, 87°, and 104° (top-down) [100]

erosion, which enhances the vortex and turbulence. All these factors strengthen the cavitation occurrence conditions. The "micro-jet" produced by bubble collapse accelerates the impact speed and cutting force of sand particles. The rough concave–convex surface caused by cavitation may increase the erosion angle of sand particles and intensify the cutting and damage of particles [85, 86]. The code GB/T 19184-2003 [87] provides the position accessible to the cavitation of the bucket.

Some scholars have studied cavitation in Pelton turbines [88–92]. They believe that most of the cavitation phenomenon can be avoided by good design, casting technology, and materials, such as cavitation-free geometry of buckets and integral casting runners [53, 93]. However, cutout region cavitation caused by high-speed jets is unavoidable. When the shape of the bucket surface changes owing to sediment abrasion, cavitation occurs on the inner surface, back surface, and outlet side of the buckets [94, 95]. To date, only a few studies
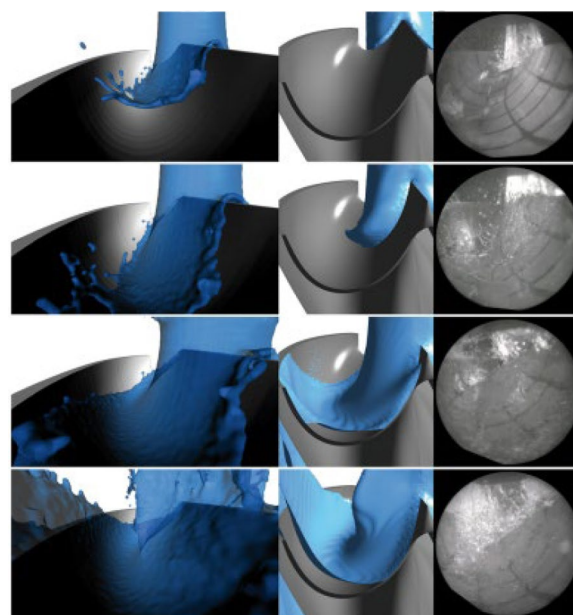
have been conducted on the combined action of sediment abrasion and cavitation on Pelton turbines [86, 94]. Therefore, further studies should be conducted on the combined effect of Pelton turbines.

4.3 Summary

The erosion of Pelton turbines is primarily caused by shear and deformation caused by impact and sliding wear. After years of development and research on wear mechanisms, erosion models have improved, but quantifying the erosion of specific parts is still challenging. The combined action of sediment and cavitation is the primary factor that causes abrasion and fatigue failure in Pelton turbines. However, research on the combined effect remains insufficient, and further studies should be conducted.

5 State-of-Art Technology of Numerical Simulation

The CFD method can be divided into Eulerian and Lagrangian methods [24, 96–99]. The Eulerian method is mature, and commercial software codes include Fluent, CFX, and OpenFOAM. However, the Lagrangian method has not been widely used because of its low accuracy. Currently, smoothed particle hydrodynamics (SPH), moving particle semi-implicit (MPS) method, and fast Lagrangian solver (FLS) are the most popular Lagrangian methods. However, the Lagrangian method has more advantages in capturing the free surface, calculating

Ge *et al. Chinese Journal of Mechanical Engineering*   (2023) 36:64

Page 11 of 27

costs, and addressing complicated geometric boundary problems [24, 96]. Figure 15 compares the two methods and the experiments used to capture the free surface. The advantage of the Lagrangian method in capturing a free surface can be observed [100, 101]. Currently, CFX is the most accurate tool in torque prediction [24] and is the most widely used, followed by Fluent. OpenFOAM requires further development because its computational cost is much higher than that of CFX and the torque is over-predicted [98]. For SPH, the Coanda effect on the back of the bucket is ignored, and the interference of the torque curve is severe, which requires further development [102, 103]. The solution speed of the FLS is the highest among all CFD methods, but the accuracy is significantly low [38]. Therefore, the FLS is only suitable for performance testing at the initial stage of runner modeling and not for optimization in the final stage [104]. The arbitrary Lagrangian–Eulerian (ALE) combines the advantages of Eulerian and Lagrangian methods and has been widely studied, but it is not yet very mature in technology [36, 96]. The MPS method [105], SPH–ALE [39, 102], and the finite volume particle method (FVPM) [106] are all new methods proposed in recent ten years, and their accuracy and applicability require improvement.

The Eulerian–Lagrangian method is the most common method for solving the Pelton turbine sediment erosion problem using CFD. The fluid is calculated using the Eulerian method, and the Lagrangian method describes the motion of solid particles. According to the different methods of interaction between the solid and fluid, it can be divided into one-way and two-way coupling. In two-way coupling, the momentum exchange term is introduced into the equation to increase the influence of particles on the flow [107]. According to Newton's second law, the empirical formula of hydrodynamic force determines the motion of particles, and particle–particle and particle–boundary interactions are not considered [16].

5.1 Numerical Simulations of Sediment Erosion
Cao et al. [108–110] studied the sediment erosion effect on a single fixed bucket (Figure 16), which differs from the actual high-speed rotating runner [111].

At least three buckets are required to study a high-speed rotating runner [112]. Kumar et al. [113] studied the influence of the sediment properties on runner erosion. Dynamic mesh technology was used in the simulation process, making the numerical simulation closer to engineering practice. Thakur et al. [71] analyzed the deformation of a runner using the finite element method. They observed that the deformation of the splitter and cutout was the largest, which was consistent with the field experiment (Figure 17).
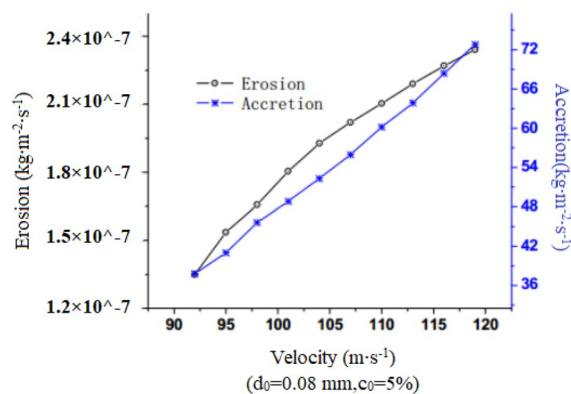

Figure 16 Erosion rate of fixed bucket [110]

Nath and Kumar [114] conducted a numerical simulation of five buckets and observed that the splitter and innermost zone of the buckets were the most vulnerable positions to erosion. Recently, Leguizamón [112, 115–118] proposed a multi-scale model to estimate the erosion rate of buckets, avoiding the limitations of commercial software relying excessively on empirical formulas. The model consisted of two sub-models: a micro-scale model and a macro model. The two sub-models were connected through sequential multi-scale coupling. The contours of the jet-bucket interaction and eroded mass are depicted in Figure 18. However, the calculation cost of this method is extremely high for it to be popularized.

Zeng et al. [119, 120] conducted a numerical simulation of the silt erosion of the injector, explored the relationship between the particle size and erosion position, and predicted the erosion characteristics of the needle. The erosion positions, particle tracks, and streamlines for different particle sizes are shown in Figure 19.

Messa et al. [121] conducted a numerical simulation study on the relationship between nozzle opening, needle tip angle, and sediment erosion. They observed that the nozzle seat and needle were the parts most easily eroded. The opening significantly impacts needle erosion, but has a slight effect on the nozzle seat. The erosion contours are shown in Figure 20. Figure 20a displays the contours of the nozzle seat following sediment erosion, while Figure 20b illustrates the contours of the needle after erosion. It is noteworthy that the nozzle seat exhibits a larger wear area and wear amount compared to the needle.

Guo et al. [122] used numerical simulations to study the erosion mechanism of the injector in depth. They considered that the secondary flow induced by the shedding of the Carmen vortex enhanced the impact velocity and impact times of the particles and strengthened the separation trend of particles, which was the main reason
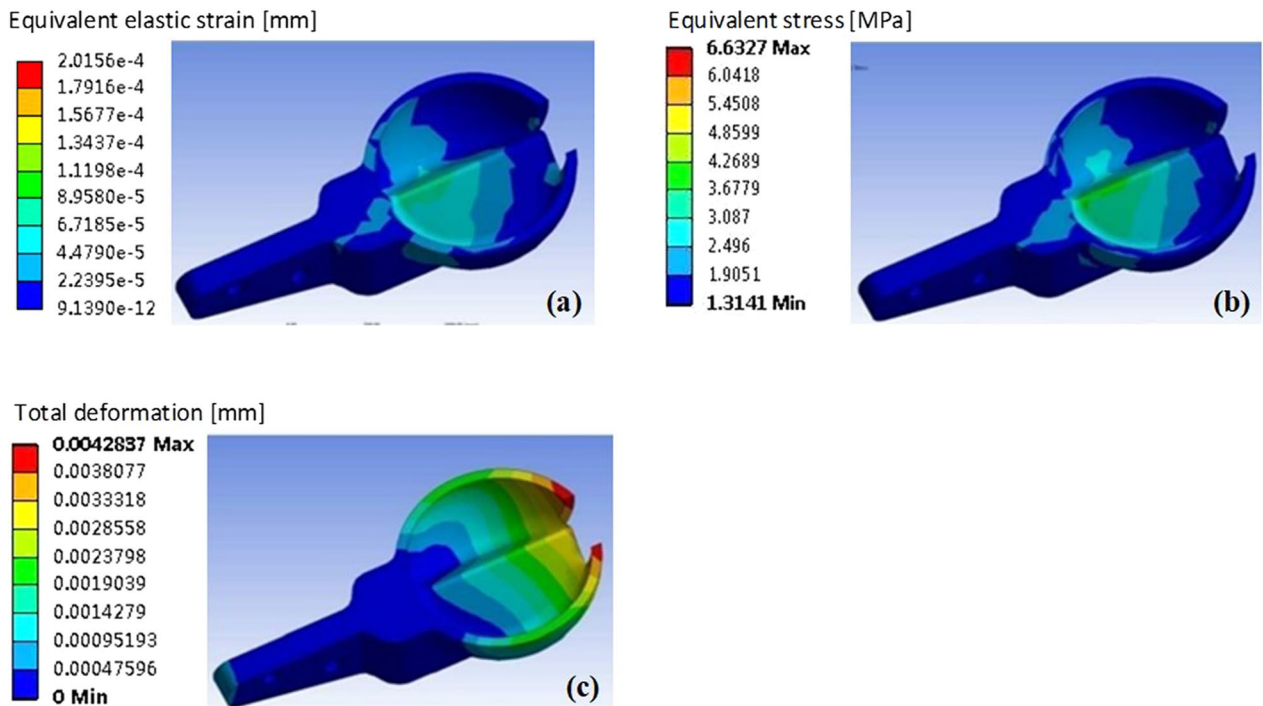
Figure 17 **a** Equivalent elastic strain on the Pelton bucket; **b** equivalent stress on the Pelton bucket; **c** total deformation in Pelton bucket
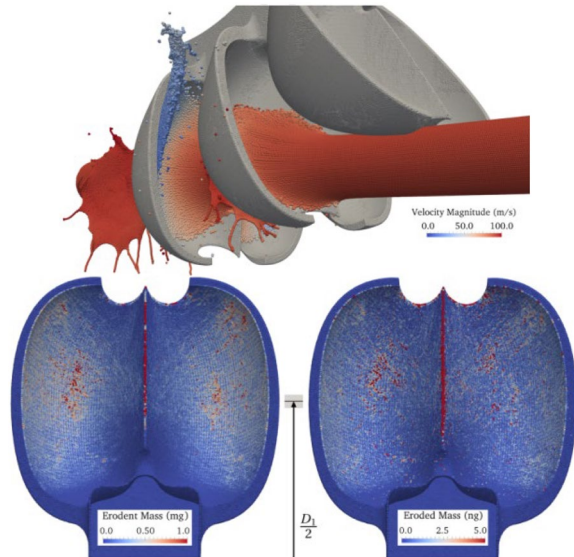

Figure 18 Contours of the jet-bucket interaction and eroded mass [112]
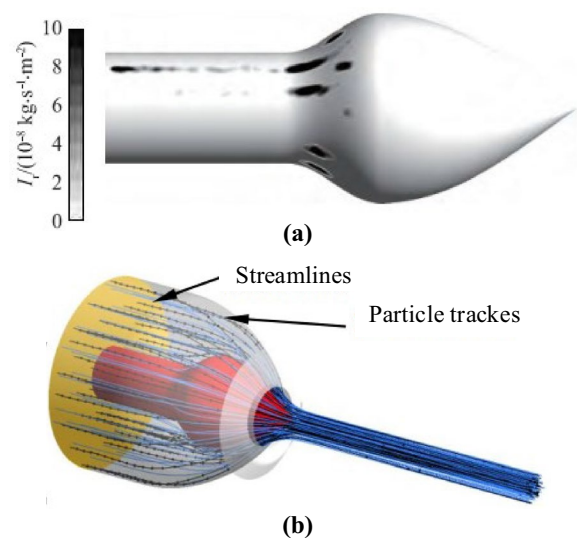
Figure 19 Erosion position of the needle under different particle sizes: **a** *D*=1 mm [119]; **b** particle tracks and streamline [120]

for the surface erosion asymmetry. The attached and extended vortex structures are shown in Figure 21.

Ge et al. [123] used the Eulerian–Lagrangian method to calculate the gas–liquid–solid three-phase unstable flow and studied the influence of the velocity and nozzle opening on the torque and erosion rate. In addition, they compared the erosion patterns and external characteristics between numerical simulations and experiments to ensure reliability. Figure 22 shows the erosion pattern of the bucket at different times under certain working conditions.

(a) Nozzle seat

(b) Needle

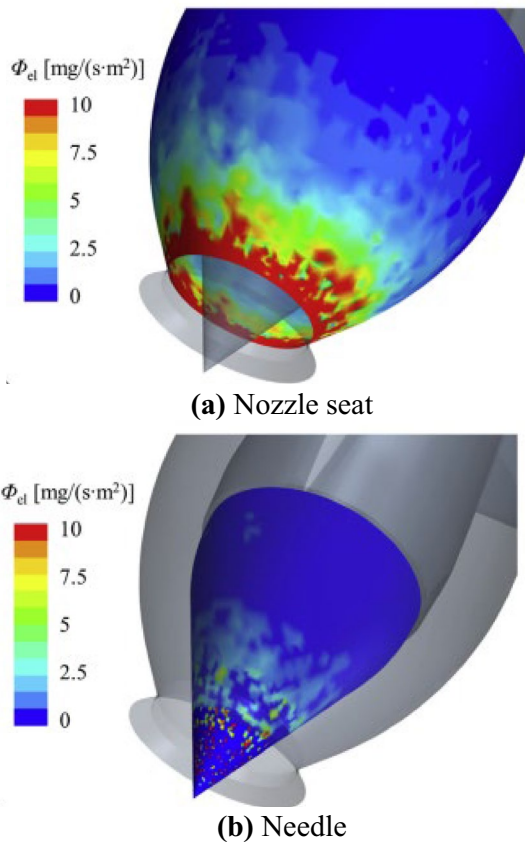**Figure 20** Erosion contours of nozzle seat and needle when γ_n=27.5, s/D_0=0.459 [121]
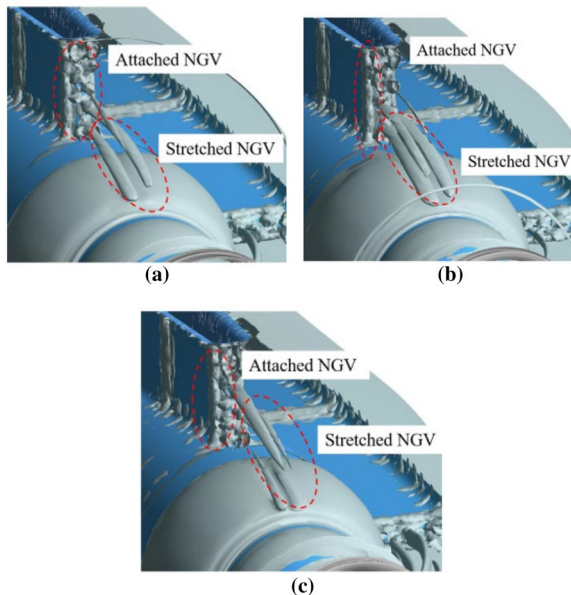
Figure 21 Vortex structure: **a** SR= 0.4; **b** SR=0.46; **c** SR= 0.54 [122]
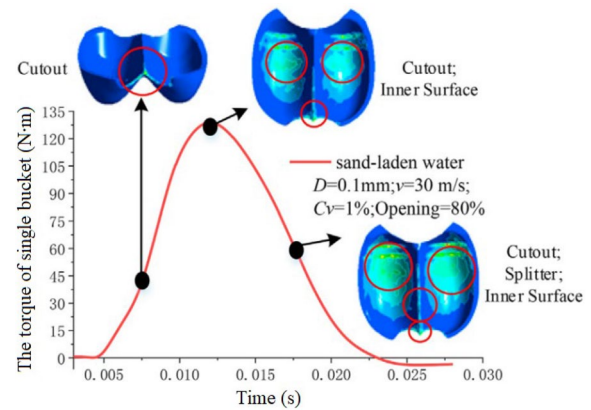
Figure 22 Erosion pattern of a bucket at different times
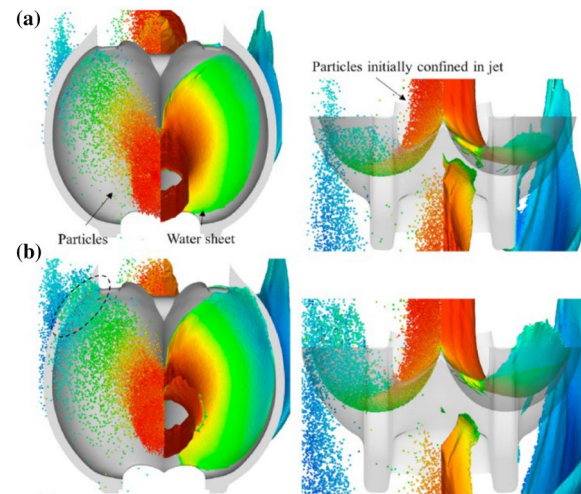
Figure 23 Particle flow patterns and water sheet colored by their absolute velocities respectively at instants: **a** 1.0 T, **b** 1.25 T

Guo et al. [124] proposed a new Eulerian–Lagrangian method and applied it for the first time to simulate the transient air–water–sediment flow in a Pelton bucket. They observed that the speed of particle separation depends largely on the curvature of the bucket, position of the particles, and speed of the water sheet. Figure 23 shows the particle flow patterns and water sheets at these instants.

5.2 Geometric Model, Boundary Conditions, and Computing Method

The injector and runner are frequently calculated separately to reduce interference factors. The computational geometry model of the injector frequently has a cylindrical jet domain such that the jet can be better and fully

Figure 24 Calculation model and boundary conditions of the nozzle [122]

Figure 25 Computational domain and boundary conditions: **a** Rotating part (red) and stationary part with six inlet regions (blue); **b** boundary conditions: walls—red, opening—yellow, symmetry—magenta, outlet—transparent blue, inlets are colored with the water volume fraction [126]

developed [119–125]. The calculation model and boundary conditions are shown in Figure 24. A structural grid or a mixed grid is often used for mesh division.
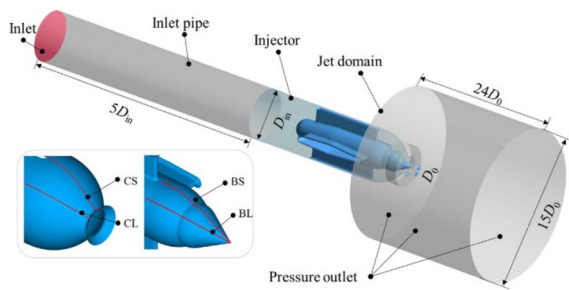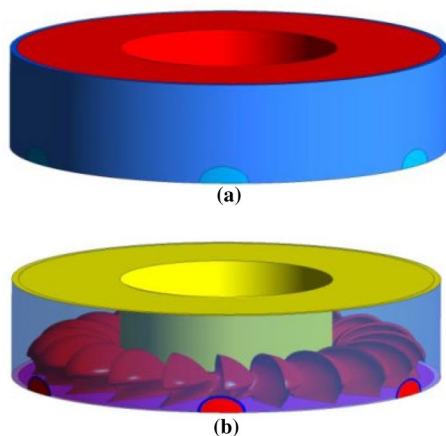
The impact of sediment particles on a runner was initially studied using a fixed bucket [108–110]. Subsequently, the calculation domain is the entire runner that is closer to the actual flow scenario. However, owing to the large number of cells, only three to five buckets are selected for numerical simulations. Some scholars use symmetric boundaries to model only half of the runner, which is not only closer to the actual scenario but also reduces the number of total cells [29, 126]. This type of symmetric modeling is more commonly used, and its calculation domain and boundary conditions are shown in Figure 25. Because of the complexity of the geometric boundary, an unstructured mesh is used. The number of cells ranges from hundreds of thousands to tens

of millions according to the differences in geometric size and calculation conditions.

Table 3 summarizes the numerical simulation method for silt erosion of Pelton turbines. The Eulerian–Lagrangian method is commonly used to simulate the silt erosion of the Pelton turbine. Other methods, such as the FVPM, have also been used to calculate sediment erosion.

5.3 Numerical Simulation Verification and Calculation Model

The verification of numerical simulation results is conducted generally through the following methods: comparison of simulation and experimental results (torque, output power, efficiency, erosion pattern), consistency analysis of the grid [130], verification of the calculation model, and comparison and analysis with reference data [113, 131, 132]. For example, Xiao [133] compared the efficiencies of experiments and numerical simulations, as shown in Figure 26. Sebastián [112] compared the prediction results with experimental values and analyzed the relative errors. Messa et al. [121] performed grid consistency analysis and two-step validation (results of reference and experimental data). To verify the accuracy and reliability of a numerical simulation, Guo et al. [122] performed the following: Based on the IEC 60193 standard, the flow rate was verified under different openings; the efficiencies of the numerical simulation and experiment were compared; the erosion patterns were compared. Figure 27 depicts the experimental validation of the erosion model. The erosion model that was compared with the numerical simulation was the Mansouri model. In an experiment, Vieira et al. [134] observed that the Mansouri model is better than the Oka, Zhang, Det Norske Veritas (DNV), and Neilson–Gilchrist models in predicting sediment erosion of bends, and it is more suitable for predicting Pelton turbine injectors.

In the numerical simulation of sediment abrasion, the main calculation models used are the multiphase flow, turbulence, particle tracking, and erosion models. The latest applications of several models are discussed below.

5.3.1 Multiphase Model

A multiphase flow model is required when the Eulerian method is used for the calculation. In ANSYS Fluent, ANSYS CFX, STAR CCM+, and OpenFOAM, based on the Eulerian method, the VOF and homogeneous multiphase models are commonly used to study Pelton turbines. The model agrees well with experimental results [135]. When the Lagrangian method is used for calculation, the multiphase flow model is not required because it simulates the flow by tracking the trajectories of particles and flow [136–138].

Ge *et al. Chinese Journal of Mechanical Engineering*　　　(2023) 36:64

Page 15 of 27

Table 3 Numerical simulation method on the silt erosion of Pelton turbines

Name	Time	Computation method	Computation object	Cells/Particles	CFD code	Computation model	Erosion model
Zeng et al. [119, 120]	2014 2015	Eulerian-Lagrangian method	Injector	2949000	Fluent	Volume of Fluid (VOF) DPM RNG *k-ε*	Finnie
Cao et al. [127]	2014	Eulerian-Lagrangian method	Injector	–	Fluent	VOF DPM Standard *k-ε*	Generic
Su et al. [108]	2014	Eulerian-Lagrangian method	One bucket	269183	Fluent	DPM Standard *k-ε*	Tabakoff and Grant
Cao et al. [109, 110]	2015	Eulerian-Lagrangian method	One bucket	915000	Fluent	DPM Standard *k-ε*	Tabakoff and Grant
Nath [128]	2017	Eulerian-Lagrangian method	Five buckets	2006527	Fluent	VOF DPM Standard *k-ε*	Generic
Messa et al. [121]	2019	Eulerian-Lagrangian method	Injector	3423114	STAR CCM⁺	VOF Lagrangian particle tracking model	Oka DNV
Sebastián et al. [112]	2020	FVPM	Three buckets	85000	–	Tait state equation Standard *k-ε*	Multi-scale erosion model
Guo et al. [122]	2020	Eulerian-Lagrangian method	Injector	3430000	Fluent	VOF DPM SST *k-ω*	Mansouri's model [129]
Ge et al. [123]	2021	Eulerian-Lagrangian method	Runner	3857916	Fluent	VOF DPM SST *k-ω*	Generic
Guo et al. [124]	2021	A new Eulerian-Lagrangian method	Injector and three buckets	2700000	Fluent	VOF DPM SST *k-ω*	–
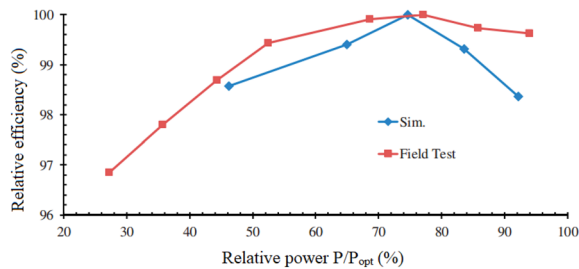
Figure 26 Verification of numerical simulations and experimental results verification [133]

Figure 27 Erosion rates comparisons along the axial direction of a pipe wall [122]

5.3.2 Turbulence Model

Three-dimensional turbulence calculations can accurately predict the actual flow of fluids [139–142]. In earlier research, the standard $k-\omega$ turbulence model was the most widely used for the Pelton turbine, and the RNG $k-\omega$ model was also used [143–148]. In recent years, scholars have recognized the SST $k-\omega$ turbulence model and widely use it to calculate high-speed turbulence for a rotating bucket. The SST $k-\omega$ turbulence model increases the influence of turbulent shear stress and has higher accuracy and credibility in the simulation of rotational shear flow at high Reynolds numbers [29, 133, 149]. Sammartano et al. [96, 150] compared the accuracy of different turbulence models in a numerical simulation of the Pelton turbine. They observed that the calculation results of the SST model were closest to the experimental values. Currently, the SST $k-\omega$ turbulence model is the most widely recognized in the Pelton turbine [151].

5.3.3 Particle Tracking Model

Owing to the sparsity of particles in sediment-laden flow, the volume fraction does not exceed 10%. The collisions between the particles are not violent and can be ignored. Therefore, the Lagrangian particle tracking model or discrete particle model (DPM) is typically used to calculate sediment particles in the flow. In the particle tracking model, inertia, drag, and gravity are the main factors considered [121, 152].

5.3.4 Erosion Model

Erosion models are often used to calculate the erosion of solid walls by particles. Different CFD codes include different erosion models. For example, the erosion models in STAR CCM$^+$ include the Ahlert, DNV, Neilson–Gilchrist, and Oka models. The erosion models in the Fluent code are the Finnie, McLaury, Oka, and generic models. The Finnie, Tabakoff, and Grant models are included in the CFX code. Other scholars have continually optimized the original model and developed new ones [153–156]. The equations for the erosion models are described as follows.

Mansouri model [134]:

$$ER = KF_S V_P^{2.41} F(\theta), \qquad (4)$$

$$F(\theta) = \frac{1}{f}(\sin\theta)^{n_1}\left(1 + HV^{n_3}(1 - \sin\theta)\right)^{n_2}, \qquad (5)$$

$$K = C(BH)^{-0.59}, \qquad (6)$$

$$BH = \frac{HV + 0.1023}{0.0108}, \qquad (7)$$

where ER is the erosion equation; F_S is the sharpness factor; $F(\theta)$ is the angle function. For SS316 (HV=1.83 GPa, BH=178.9) and 300 μm sand, the values of C and K are 4.62×10^{-7} and 2.16×10^{-8}, respectively.

Oka model [153]:

$$ER = ER_{90} g(\theta), \qquad (8)$$

$$ER_{90} = K_P(H_V)^{k_1}(V_P)^{k_2}(d_P)^{k_3}, \qquad (9)$$

$$g(\theta) = (\sin\theta)^{n_1}(1 + H_V(1 - \sin\theta))^{n_2}, \qquad (10)$$

where k_1 and k_3 are empirical exponent factors; k_2 is a function of the material hardness and particle properties; K_P is an independent factor that denotes particle properties, such as shape and hardness; H_V is the Vickers hardness.

Zhang model:

$$ER = 2.17 \times 10^{-7}(BH)^{-0.59} F_S V_P^{2.41} F(\theta), \qquad (11)$$

$$F(\theta) = 5.4\theta - 10.11\theta^2 + 10.93\theta^3 - 6.33\theta^4 + 1.42\theta^5, \qquad (12)$$

where θ is the particle incidence angle; BH is the Brinell hardness of the eroded material; F_S is the sharpness factor.

DNV model [80]:

$$\begin{cases} ER = \dot{m}_P K_N V_P^{n_N} F(\theta), \\ f(\theta) = \sum_{i-1}^{8} (-1)^{i+1} A_i \left(\frac{\theta\pi}{180}\right)^i, \end{cases} \qquad (13)$$

where $\dot{m}_P$ is the mass rate of solid particles; K_N and n_N are the material constants ($K_N = 2.0 \times 10{-9}$, $n_N = 2.6$ for steels); A_i is a model constant.

Neilson–Gilchrist model [157]:

$$ER = ER_C + ER_D, \qquad (14)$$

$$ER_C = \begin{cases} \dfrac{V_P^2 \cos^2\theta \sin\frac{n\theta}{2\theta_0}}{2e_C}, & \theta < \theta_0, \\ \dfrac{V_P^2 \cos^2\theta}{2\varepsilon_C}, & \theta < \theta_0, \end{cases} \qquad (15)$$

$$ER_D = \frac{\max(V_P \sin\theta - K_D, 0)^2}{2\varepsilon_D}, \qquad (16)$$

where ER_C and ER_D are the contributions of cutting and deformation, respectively; θ_0 is the transition angle, normally set as 45°; ε_C is the cutting coefficient, 3.332×10^7; ε_D is the deformation coefficient, 7.742×10^7; K_D is the cutoff velocity.

All models consider the particle's reflection on the geometric walls, which depends on the properties of the particles and the surface of the solid. Therefore, erosion models are empirical or semi-empirical formulas based on numerous experiments [153, 154, 158]. The Finnie model is the most widely used model, but it often results in the over-prediction of erosion [128, 159]. Messa et al. [160, 161] studied the influence of different erosion models and parameters on the erosion rate. They observed that erosion results were highly dependent on these empirical or semi-empirical erosion models.

5.4 Summary

From a development perspective, this section comprehensively introduces numerical simulation methods, geometric model structures, boundary conditions, and calculation methods.

In the numerical simulation of the sediment erosion of the Pelton turbine, many simplifications are required; therefore, some uncertainties exist [8]. The accuracy of erosion prediction is based on the following two points: the erosion position, which can be obtained by comparing it with the eroded parts. The other is the erosion rate, which challenges the existing technology [112].

The accuracy of numerical simulations encounters significant challenges because many values are assumed under ideal conditions. Not all processes of sediment erosion can be realized using CFD, such as coating erosion, shear deformation of the substrate material after coating removal, and secondary cavitation caused by erosion [17]. In addition, secondary flow is difficult to simulate, and the problems of turbulence and inaccurate boundary conditions are difficult to avoid [38]. Accurate modeling of centrifugal and Coriolis forces is also a problem in CFD [162]. Finally, owing to the unsteady characteristics of the calculation, the calculation ability requirement is higher. All these factors result in inaccuracies in the simulation results. The cavitation phenomenon of Pelton turbines using CFD has been studied, but only a few studies have been conducted on the combined erosion of cavitation and sediment [90, 126, 163].

In addition to those mentioned above, the numerical simulation results depend on the erosion model used. Currently, no complete or standard erosion model is available [128].

Therefore, studying a general and valuable erosion model will be crucial and challenging in the future. In addition, obtaining a similarity between a model and an actual unit with respect to sediment erosion conditions is difficult. Therefore, dynamic similarity criteria and formulas should be established in the future [112].

6 Protection Measures for Sediment Erosion

6.1 Anti-Erosion Design

Anti-erosion design primarily includes the design of hydraulic structures and hydraulic turbines. The main direction of the optimization design of hydraulic structures is to reduce the sediment concentration of the flow through the turbine [164]. Several designs of hydraulic structures are introduced as follows.

a. Sediment trapping systems
   As early as 1911, Dufour applied a sediment trapping system to a reaction turbine power station [17]. In 1919, sand traps were used at an impact turbine power station, and the effect proved useful [17]. For example, after applying the desilting basin in a CCS power station, the actual effect was satisfactory [165]. Sand trapping was also built to solve the problem of excessive sediment at the Chilime Power Station.

However, during flooding, its role is minimal [50], and its control effect on fine silt is poor [166].

b. Installation can include additional low-head weirs in the entire tributary upstream of power stations [49].

c. The layout of the hydro project should be planned reasonably, and the unit should be arranged at a position conducive to reducing sediment passing through the turbine [22].

d. Increase the sediment settling effect of the reservoir and design a multi-stage sediment reduction and desilting design system [165, 167].
   The structural design of Pelton turbines is the most important because the most easily eroded parts determine the maintenance period [10]. The primary method to optimize the structural design is to reduce the velocity and optimize the impact angle [10]. The ultimate goal of the design optimization is to achieve minimum erosion and maximum efficiency [168]. The selection of the design parameters of Pelton turbines in a high-sediment-laden river can be based on the following standards:

e. Low-velocity inlet design [15]. S_W(silt concentration)<5 kg/m^3, U_2 or W_2<38–40 m/s; S_W(silt concentration)<12 kg/m^3, U_2 or W_2<34 m/s [169] (The velocity is related to the material of the flow passage parts).

f. When the nozzle outlet velocity is large ($\geq$ 150 m/s), the contact surface between the nozzle and needle in the closed position should be as small as possible ($\leq$ 1 mm) [15]. The nozzle tip should be as sharp as possible [49].

g. In the design, the separation angle between the particles and the streamline should be reduced [84].

h. The bucket curvature, hydraulic radius, and nozzle hydraulic radius should be increased [170].

6.2 Wear-Resistant Materials, Manufacturing Technology, and Other Protection Measures

Fatigue failure and fracture of the Pelton turbine runner caused by wear severely affects the safe operation of the power station. The anti-abrasion design can effectively reduce the sediment concentration of the flow through the turbine; however, its effect is limited. Here, the reasonable selection of anti-resistant materials and manufacturing technology will significantly affect the protection.

6.2.1 Runner Materials

The early runner material was generally cast iron [17]. In 1934, the advantages of stainless steel were demonstrated [171]. After continuous exploration and development, 13Cr4Ni has become a standard material for turbine

parts [73]. Hardness, toughness, and elasticity are essential indices for evaluating the wear resistance of materials [172]. Traditional cast stainless steel (SCSI, SCS5, and SCSI3), high-nickel, high-manganese chromium stainless steel (NMC and NMW), and high-carbon steel (DFME) exhibit good wear resistance [15]. In recent years, forged stainless steel has been proven to have excellent properties, particularly integrally forged stainless steel, which has almost no casting defects and strong fatigue resistance [173, 174]. Increasing surface hardening is also a more effective method of addressing wear [88]. However, the specific material selection should comprehensively consider the wear strength, environmental temperature, corrosion, impact load, static load, total cost, service life, functional requirements, available manufacturing equipment, and other factors [175–178].

6.2.2 Hard Coating
After 1980, researchers began to realize the role of coatings in resisting substrate erosion. The actual operation of a power plant has shown that the coating can effectively reduce the erosion rate [10, 54, 179]. Coatings are generally divided into three types: hard, elastomer, and composite [180]. Common coating and process methods include WC series cermet coating and high-velocity oxyfuel spraying (HVOF) [10, 17, 181, 182]. In addition, nano-coating [183], plasma spraying, rubber coating [15], boronizing coating [128], tungsten carbide coating [174], stainless steel coating [184] and non-metallic coating [185, 186] have strong wear resistance. In the selection of the coating type, the combination of coating and surface material, the performance of the coating, and the coating method should be considered comprehensively because they jointly determine the corrosion resistance of the coating [187].

6.2.3 Manufacturing Technology
Good manufacturing technology can avoid damage to runners to the greatest extent. The leading manufacturing technologies of hydraulic turbines include investment casting, sand casting, numerical control (NC) machining, and forging. Currently, most hydraulic turbine manufacturers worldwide use NC machining technology to manufacture hydraulic turbines [188, 189]. The companies Voith (Germany), ABB (Switzerland), VA (Austria), and ALSTOM (France) have mastered the advanced manufacturing technology of Pelton turbines [190]. The typical manufacturing technologies for Pelton turbines are integral casting [191, 192], MicroGuss^{TM}, and complete forging [193]. The structural optimization design of the Pelton turbine high-stress zone, casting process simulation, and deep cooperation between the manufacturing industry and academia will contribute to further improvements in manufacturing technology [188, 194].

6.2.4 Control of Operation Process and Maintenance
Based on anti-erosion design and wear-resistant material selection, regular maintenance and repair are necessary. Such a non-destructive test (DNT), which includes the dye penetration test (DPT) and magnetic particle test (MPT), has been used to detect the flow channel [195, 196]. Some operation control measures are frequently implemented to protect unit safety during a high sediment period, for example, an outage in the high sediment period [197]; in the monsoon season, the flow is reduced by diversion [49].

The methods mentioned above require the installation of real-time monitoring devices in a power station. The monitoring system evaluates the sediment condition, and then determines the operating strategy of the power station.

6.3 Summary
This section introduces the general protection measures for sediment erosion in detail, including the power station layout, hydraulic structure design, manufacturing technology, anti-wear materials, and maintenance. The structural optimization of the flow passage components and an in-depth study of anti-wear materials are still critical challenges for the future. Cooperation between the manufacturing industry and academic community can also further improve anti-wear technology.

Erosion prediction and fault diagnosis technologies are useful for structural optimization design, material selection, operation range selection, and repair work (see Section 7).

7 Monitoring and Prediction Technology of Sediment Erosion
The water conditions of the river can be obtained from hydrological observation data collected over many years. Before installing the unit, the erosion of the buckets can be estimated, and the positions accessible to erosion should be protected in the material selection and design stage. In addition, reliable and systematic monitoring of turbine erosion and efficiency, and a complete record of maintenance and associated costs can optimize the operation of hydropower stations in terms of profitability and generation capacity [197]. Therefore, a sediment monitoring system, erosion measurement, and prediction technology are essential.
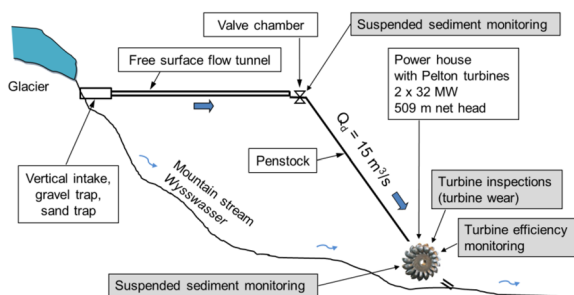
Figure 28 Schematic of a hydropower station research project [194]

(a) Needle   **(b)** Nozzle seat

Figure 29 Nozzle seat and needle after erosion [49]

Figure 28 shows a typical structural diagram of a power station monitoring system [198], which primarily includes monitoring of suspended sediment, inspection of bucket erosion, and monitoring of external characteristics of hydraulic turbines.

This section introduces the erosion detection technology for Pelton turbines, sediment characteristic measurement technology, and fault diagnosis technology. Advanced monitoring technology can ensure the benefits of hydropower stations, extend the service life of flow passage components, and provide better maintenance and scheduling [199].

7.1 Erosion Detection Technology of Buckets

In the laboratory, erosion loss is primarily expressed by mass loss, thickness changes, and surface roughness changes [166]. Generally, the size of the tested part is small; therefore, it is easy to measure [62]. Probes, thickness gauges, and mechanical calipers are commonly used as the traditional measuring instruments. However, traditional measuring instruments have difficulties measuring small erosion thickness changes. Recently, new measurement methods have been proposed. The following are several methods for measuring erosion.

7.1.1 3D-scanner

A three-dimensional (3D) scanner is often used to quantify the erosion of the bucket surface, which is primarily composed of an LED and cameras [62]. A 3D scanner is the most advantageous of all surface detection technologies because it can measure the erosion depth, blade profile, and material loss [62]. During the monitoring, some reference points will be made on the surface to better observe the change in the blade surface after erosion. The advantage of this method is that it can accurately monitor surface erosion; however, the scanning time is excessively long [8].

Parray [49] used 3D scanning technology to evaluate the erosion of the needle (Figure 29a) and nozzle seat (Figure 29b) of a power station operating for 2712 h.
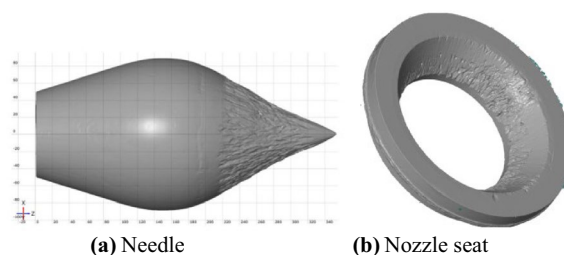
The accuracy of the 3D scanner was 10 μm and the scanning range was 500 mm. According to this assessment, the nozzle and needle erosion rates were 3.71% and 5%, respectively. The surface of the needle and nozzle seat after sediment erosion can be clearly observed in Figure 29a and b, respectively, using 3D scanning. The results show the presence of scratches and pits on the surface of both components. Morales [200] conducted a 3D scanning of the bucket surface, the results of which are shown in Figure 30.

7.1.2 Imaging and Video Techniques

The advantages of imaging and video techniques are that large-scale disassembly is not required, the detection time is short, and the images can be compared offline [54, 62], such as through visualization technology and digital image processing. Visualization technology is a simple and effective tool for testing models. It can be used to analyze the interaction between the water flow and runner [201, 202], and it can also be used to diagnose the noise of prototype units [203]. It has been applied at Moccasin and other power plants [204]. Digital image processing technology is often combined with MATLAB to measure the final erosion profile of the buckets. Shrestha [166] used this technology to study Pelton turbines. The runner was operated continuously for 72 h in a sediment-laden flow, and the bucket profile was repeatedly measured ten times. The results showed that this method can accurately and quantitatively detect the erosion of sharp edges.
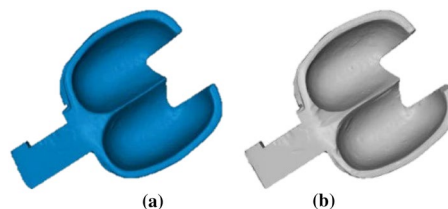

(a)   **(b)**

Figure 30 Surfaces of the bucket: **a** Before erosion; **b** after erosion [200]

Figure 31 Check the shape of the bucket after maintenance using a template [191]
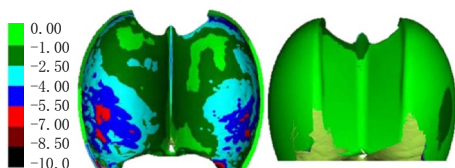

Figure 32 Variation in sediment erosion depth on the front and back of the bucket [205]
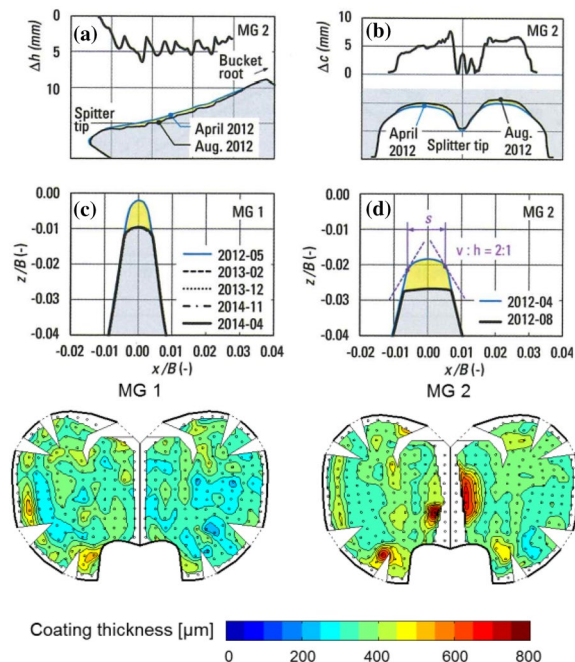

Figure 33 Profile change and coating thickness change of buckets [54, 197, 198]

7.1.3 Template Inspection

The IEC recommends using a template to measure the erosion thickness of uncoated buckets [73]. This method can effectively detect changes in the shape of the bucket, as shown in Figure 31. However, quantifying the erosion of each part of the bucket is impossible, particularly the cutout position [62].

7.1.4 Thickness Gauge Based on Magnetic Induction

Thickness gauges are often used in conjunction with 3D scanning to quantify the erosion. The variation in the erosion depth of the bucket after 3180 h of operation of a 10 MW hydropower station in India is shown in Figure 32 [205]. Three years of measurement at the Fieschertal power station was used to analyze the erosion of buckets with a hard coating. The profile changes at the splitter and cutout and thickness changes in the bucket coating are shown in Figure 33 [54, 197, 198].

7.2 Measurement Technology of Sediment Characteristic Parameters and Fault Diagnosis Technology

Erosion results are affected by the concentration, size, shape, and mineral composition of the sediment. In the monsoon season, the sediment concentration and particle size distribution in the river frequently vary significantly. Hence, the power station must track the changes in suspended sediment concentration (SSC) and particle size distribution (PSD) over time. However, the particle shape and mineral composition of the sediment do not change in a short period, which does not require real-time monitoring. Gravity analysis, vibrating tube density, turbidity, acoustic attenuation, laser diffraction, and acoustic backscatter are commonly used to measure the SSC and PSD [62, 206–209]. SSC and PSD measurements are introduced below.

7.2.1 SSC Measurement

The traditional measurement method for SSC is to collect samples and conduct laboratory analyses [210]. However, when extreme weather, such as a rainstorm, occurs, many samples are often required, and the cost is very high [211–213]. In recent years, continuous measurement technology (CMT) based on turbidity, acoustics, lasers, and pressure differences has attracted increasing interest [208]. The combined application of measurement and CMT technology based on spectral reflection and
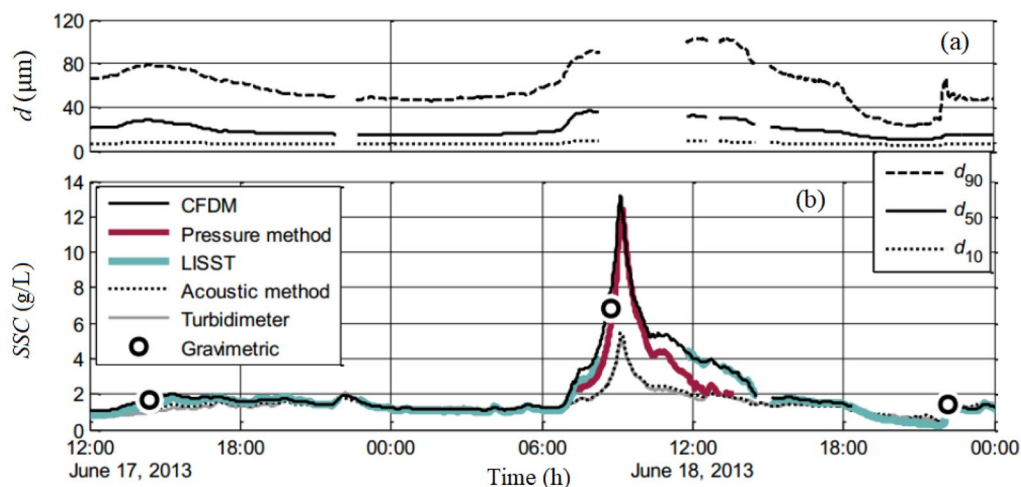
Figure 34 Comparison of the SSC and PSD measurement results of different methods: **a** Particle sizes obtained from LISST; **b** SSCs from six techniques, measured in the valve chamber of Fieschertal HPP [218]

image capture is a future development trend [208, 214, 215]. Although CMT has many apparent advantages over traditional measurement methods, it is affected by calibration, reliability standards, and microbial fouling. In future development, more research should be conducted to improve measurement accuracy, scope, and applicability. Further analysis of the relationship between sediment concentration and turbidity can be used to effectively detect water quality at the inlet [216, 217].

7.2.2 Measurement of PSD
The commonly used measurement methods for PSD are dynamic imaging (Camsizer) and laser diffraction (LISST) [49]. Some technical equipment, such as a multi-frequency acoustic instrument for monitoring, has been applied at the Toss power station, which can continuously monitor the SSC and PSD [114, 205]. Figure 34 compares the SSC and PSD measurement results of different methods [218].

7.2.3 Fault Diagnosis Technology of Condition Monitoring
There are three main types of damage: fatigue, sediment erosion, and cavitation [219]. Through monitoring and diagnosis, symptoms can be observed in the early stages of damage to reasonably plan the maintenance cycle or estimate unit life. Some scholars have studied this problem in recent years, but only a few references are available [220, 221]. The general monitoring and diagnosis technology method monitors the vibration, analyzes the vibration spectrum, and then determines the damage type and position by comparing it with the database. However, the Pelton turbine lacks historical cases and databases, and its applications are limited. Egusquiza

et al. [173] collected the operation data of 28 Pelton turbines over 25 years, analyzed the database, and extracted different damage types. Åsnes [222] collected data from 27 power stations and used three methods to diagnose the Pelton turbines.

8 Conclusion and Prospects
The sediment carried by a high-head flow has high kinetic energy, severely damaging the flow passage parts of Pelton turbines. As plant manufacturers and scholars gain more interest the benefits, safety, and stability of hydropower station operations, many countries spend significantly to solve the problem of hydro-abrasive sediment erosion. With the development in recent years, engineering design and sediment reduction measures have become increasingly mature, and sediment concentration has been dramatically reduced. Experiments and case analyses have revealed the relationship between silt and unit erosion and external characteristics, and many erosion models have been established. However, owing to the complexity of flow, the influence of specific erosion parameters remains difficult to distinguish. Experimental research also has some limitations in solving this problem, such as excessively long erosion observation periods and limited experimental conditions.

With improvements in computing power and technology development, CFD has received increasing interest as a research method. CFD can model the Pelton turbine successfully, simulate the flow pattern of sediment-laden flow in the operation process, and be used to study a three-dimensional unsteady erosion on nozzles, needles, and runners. However, CFD has limitation, such as erosion prediction, over-reliance on empirical or

semi-empirical formulas, and a lack of calculation of secondary flow and secondary cavitation. The development of a complete and valuable syndication erosion model, establishment of dynamic similarity criteria and similarity formulas, improvement of computational capability, and optimization of the calculation method are the development directions of CFD in the future.

The casting process and material selection are the key factors that determine the performance of a runner. In recent years, rapid progress has been achieved in technology that has significantly improved the erosion resistance of runners. In the future, an in-depth study of anti-erosion materials will be essential for technological development. Therefore, a better combination of science and engineering is required for the research and development, optimization, design, and manufacturing of hydraulic machinery. In addition, advanced monitoring technology can ensure the benefits of the power station, extend the service life of the flow passage components, and provide better maintenance scheduling. This paper discusses the development and latest progress in research on sediment erosion, which provides some references for technical researchers in related fields.

Abbreviations

CFD	Computational fluid dynamics
SPH	Smoothed particle hydrodynamics
MPS	Moving particle semi-implicit
FLS	Fast Lagrangian solver
FVPM	Finite volume particle method
HPP	Hydro Power Plant
SSC	Suspended sediment concentration
DNT	Non-destructive test
MPT	Magnetic particle test
ALE	Arbitrary Lagrangian–Eulerian
HVOF	High-velocity oxyfuel spraying
SSC	Suspended sediment concentration
PSD	Particle size distribution
CMT	Continuous measurement technologies
NC machining	Numerical Control Machining
PSD	Particle size distribution
DPT	Dye penetration test
VOF	Volume of fluid

Authors' Information
Xinfeng Ge, born in 1981, is currently a lecturer at *College of Energy and Electrical Engineering, Hohai University, China*. He received his PhD degree from *China Institute of Water Resources and Hydropower Research, China,* in 2011. His research interests include fluid machinery multiphase flow and large equipment fault diagnosis. E-mail: gexinfeng@hhu.edu.cn
Jie Sun, born in 1995, is currently a PhD candidate at *College of Water Conservancy and Hydropower Engineering, Hohai University, China*. E-mail: sunjie_@hhu.edu.cn
Dongdong Chu, is currently a research fellow at *Jiangsu Water Conservancy Research Institute, China*. E-mail: bwhhxq@163.com
Juan Liu, is currently a research fellow at *China Institute of Water Resources and Hydropower Research, China*. E-mail: liujuan@iwhr.com.cn
Ye Zhou, is currently a research fellow at *China Institute of Water Resources and Hydropower Research, China*. E-mail: zhouye@foxmail.com
Hui Zhang, is currently an engineer at *Chongqing Shipping Construction Development Co., Ltd., China*.
Lei Zhang, is currently an engineer at *Yellow River Institute of Hydraulic Research, China*.
Huixiang Chen, born in 1989, is currently an associate professor at *College of Agricultural Science and Engineering, Hohai University, China*. E-mail: chenhuixiang@hhu.edu.cn
Kan Kan, born in 1990, is currently an associate professor at *College of Energy and Electrical Engineering, Hohai University, China*. E-mail: kankan@hhu.edu.cn
Maxime Binama, is currently a post-doctoral at *College of Water Conservancy and Hydropower Engineering, Hohai University, China*. E-mail: binamamaxime@hhu.edu.cn
Yuan Zheng, born in 1964, is currently a professor at *College of Energy and Electrical Engineering, Hohai University, China*. E-mail: zhengyuan@hhu.edu.cn

Data availability
The data used to support the findings of this study are included within the article.

Declarations

Competing Interests
The authors declare no competing financial interests.

References
[1] IHA, 2019 Hydropower Status Report-Sector Trends and Insights. UK, 2019.
[2] 2019 Annual Report of China Hydropower information. China Society for Hydropower Engineering, 2019. (in Chinese)
[3] Ministry of Water Resources of the PRC. Bulletin of River Sediment in China, 2019. (in Chinese)
[4] B Shrestha, B Gautam, T Bajracharya. Computational analysis of Pelton bucket tip erosion using digital image processing. *Electronic Imaging & Multimedia Technology V*, 2007, 6833: 825-835.
[5] M K Padhy, R P Saini. Effect of size and concentration of silt particles on erosion of Pelton turbine buckets. *Energy*, 2009, 34(10): 1477-1483.
[6] M K Padhy, R P Saini. Study of silt erosion on performance of a Pelton turbine. *Energy*, 2011, 36(1): 141-147.
[7] B Thapa, R Shrestha, P Dhakal, et al. Problems of Nepalese hydropower projects due to suspended sediments. *Aquatic Ecosystem Health & Management*, 2005, 8(3): 251-257.
[8] A K Rai, A Kumar, T Staubli, et al. Interpretation and application of the hydro-abrasive erosion model from IEC 62364 (2013) for Pelton turbines. *Renewable Energy*, 2020, 160: 396-408.

[9]   B Thapa, R Shrestha, P Dhakal, et al. Sediment in Nepalese hydropower projects. *Proc. Int. Conf. on the Great Himalayas: Climate, Health, Ecology, Management and Conservation*, 2004.

[10] K Winkler. Hydro-abrasive erosion: Problems and solutions. *IOP Conference Series Earth and Environmental Science*, 2014, 22(5): 052022.

[11] M K Padhy, R P Saini. A review on silt erosion in hydro turbines. *Renewable & Sustainable Energy Reviews*, 2008, 12(7): 1974-1987.

[12] J L Liu. Discussion on the harm of sediment to turbine operation in Gezhouba Hydropower Station. *Yangtze River*, 1982, (04): 85-91. (in Chinese)

[13] L Lu, J Liu, Y L Yi, et al. Evaluation on sand abrasion to Baihetan hydraulic turbines. *Journal of Hydroelectric Engineering*, 2016, 35(02): 67-74. (in Chinese)

[14] Y W Shi. *Study of sand-mud abrasion, cavitation damage and their protections for the turbines of the Sanmenxia Hydropower Station*. Nanjing: Hohai University, 2006. (in Chinese)

[15] C G Duan, V Y Karelin. *Abrasive erosion and corrosion of hydraulic machinery*. London: Imperial College Press, 2002.

[16] S Sangal, M K Singhal, R P Saini. Hydro-abrasive erosion in hydro turbines: A review. *International Journal of Green Energy*, 2018, 15(4): 232-253.

[17] D Felix, I Albayrak, A Abgottspon, et al. Hydro-abrasive erosion of hydraulic turbines caused by sediment-a century of research and development. *The 28th IAHR Symposium on Hydraulic Machinery and Systems*, 2016: 122001.

[18] B S Thapa, O G Dahlhaug, B Thapa. Sediment erosion in hydro turbines and its effect on the flow around guide vanes of Francis turbine. *Renewable & Sustainable Energy Reviews*, 2015, 49: 1100-1113.

[19] L Kumar, C Parashar, S Kaur. Prediction of silt erosion in hydraulic turbine using non-linear regression model. *IJESR*, 2013, 4: 963-970.

[20] B Thapa. *Sand erosion in hydraulic machinery*. Trondheim: Norwegian University of Science and Technology Norway, 2004.

[21] M Sallaberger, H Keck, A Heimann, et al. Comparing recent technology for high head francis and multi-jet pelton turbines. *International Journal on Hydropower & Dams*, 2009, 16(1): 77.

[22] Y Zeng, S Y Fan. Type selection, hydraulic design and structure optimization of turbine for sediment-laden power station. *Mechanical & Electrical Technique of Hydropower Station*, 2013, 36(2): 1-6+63. (in Chinese)

[23] M V Casey, H Keck. *Hydraulic turbines*. Handbook of Fluid Dynamics and Fluid Machinery, 1996.

[24] A Židonis, G A Aggidis. State of the art in numerical modelling of Pelton turbines. *Renewable and Sustainable Energy Reviews*, 2015, 45: 135-144.

[25] L A Pelton. Water Wheel. U.S. Patent No. 233,692. Washington, DC: U.S. Patent and Trademark Office, 1880.

[26] T Staubli, A Abgottspon, P Weibel, et al. Jet quality and Pelton efficiency. *Hydro*, 2009: 26-28.

[27] Z Zhang. Flow friction theorem of Pelton turbine hydraulics. *Proceedings of the Institution of Mechanical Engineers-Part A Journal of Power & Energy*, 2007: 1173-1180.

[28] D S Benzon. *The Turgo impulse turbine: a CFD based approach to the design improvement with experimental validation*. Lancaster: Lancaster University, 2016.

[29] C J Zeng. *Research on the internal flow characteristics and flow interference of Pelton turbine*. Beijing: Tsinghua University, 2018. (in Chinese)

[30] B Nasir. Design of high efficiency Pelton turbine for microhydropower plant. *Int. J. Electr. Eng. Technol.*, 2013, 4: 171-183.

[31] J Anagnostopoulos, D Papantonis. A numerical methodology for design optimization of Pelton turbine runners. *Hydro*, 2006: 25-27.

[32] K Patel, B Patel, M Yadav, et al. *Development of Pelton turbine using numerical simulation*. IOP Conference Series: Earth and Environmental Science, 2010, 12(1): 012048.

[33] A A Fulton. Present tendencies in water turbine machinery. *ARCHIVE Proceedings of the Institution of Mechanical Engineers*, 1937, 135: 387-444.

[34] M Nechleba. *Hydraulic turbines, their design and equipment*. Penerbit Artia, 1957.

[35] Z J Zhang. Development and new technology of Pelton turbines. *Large Electric Machine and Hydraulic Turbine*, 2017, 4: 1-6. (in Chinese)

[36] A Rossetti, G Pavesi, G Cavazzini, et al. Influence of the bucket geometry on the Pelton performance. *Proceedings of the Institution of Mechanical Engineers, Part A: Journal of Power and Energy*, 2014: 33-45.

[37] A Židonis, G A Aggidis. Pelton turbine: Identifying the optimum number of buckets using CFD. *Journal of Hydrodynamics*, 2016, 28(1): 75-83.

[38] J Anagnostopoulos, P Koukouvinis, F Stamatelos, et al. Optimal design and experimental validation of a turgo model hydro turbine, engineering systems design and analysis. *American Society of Mechanical Engineers*, 2012: 157-166.

[39] M Rentschler, J C Marongiu, M Neuhauser, et al. Overview of SPH-ALE applications for hydraulic turbines in andritz Hydro. *Journal of Hydrodynamics*, 2018, 30(1): 114-121.

[40] Stromanbieterwechsel, Ökostrom. (2023-3-20) http://www.stromanbieterwechsel.net/oekostrom.html, 2017-10-03.

[41] Z Zhang. *Pelton turbines*. Switzerland: Springer International Publishing, 2016.

[42] S H Gu. A review on turbine abrasion. *Symposium on Anti-Abrasion Technology of Hydraulic Turbine*, Lanzhou, China, 2006: 37-42. (in Chinese)

[43] D Felix. *Experimental investigation on suspended sediment, hydro-abrasive erosion and efficiency reductions of coated Pelton turbines*. Swiss: ETH Zurich, 2017.

[44] J Liu, J Yu, C Jiang. Evaluation on sediment erosion of Pelton turbine flow passage component. *IOP Conference Series: Earth and Environmental Science*, Institute of Physics Publishing, 2019, 240(2): 022027.

[45] A K Rai, A Kumar, T Staubli. Effect of concentration and size of sediments on hydro-abrasive erosion of Pelton turbine. *Renewable Energy*, 2020, 145: 893-902.

[46] A K Rai, A Kumar, T Staubli. Analytical modelling and mechanism of hydro-abrasive erosion in pelton buckets. *Wear*, 2019, 436-437: 203003.

[47] F Avellan, P Dupont, S Kvicinsky, et al. Flow calculations in Pelton turbines- Part 2: Free surface flows. *Proceedings of the 19th IAHR Symposium on Hydraulic Machinery and Cavitation*, Singapore, Republic of Singapore. Vol. 1. No. CONF. International Association for Hydraulic Research, 1998: 294-305.

[48] A Rai, A Kumar, T Staubli. Developing a test rig to measure hydro-abrasive erosion in Pelton turbine. *International Conference on Hydropower for Sustainable Development*, 2015: 535-547.

[49] M Z U Din, G A Harmain. Assessment of erosive wear of Pelton turbine injector: Nozzle and spear combination - A study of Chenani hydropower plant. *Engineering Failure Analysis*, 2020, 116:104695.

[50] T R Bajracharya, B Acharya, C B Joshi, et al. Sand erosion of Pelton turbine nozzles and buckets: A case study of Chilime hydropower Plant. *Wear*, 2008, 264(3): 177-184.

[51] M Colley, R Connell, J Firth, et al. Climate risk case study: first Khimti hydropower scheme Himal Power Limited, Nepal. *The World Bank*, 2011, 62639: 1-136.

[52] D H Hu, F He, Z F He, et al. Anti-sediment abrasion design of turbine at Zhala Hydropower Station. *Yunnan Water Power*, 2019, 35(1): 128-130+134. (in Chinese)

[53] W T Zhou, X Q Zhou.The runner bucket damage of Pelton turbine. *Large Electric Machine and Hydraulic Turbine*, 2006, 6: 47-50. (in Chinese)

[54] A Abgottspon, T Staubli, D Felix. Erosion of Pelton buckets and changes in turbine efficiency measured in the HPP Fieschertal. *The 28th IAHR Symposium on Hydraulic Machinery and Systems*, 2016, 49(12): 122008.

[55] A K Rai, A Kumar, T Staubli. Financial analysis for optimization of hydropower plants regarding hydro-abrasive erosion: A study from Indian Himalayas. *IOP Conference Series: Earth and Environmental Science*, IOP Publishing, 2019, 240(2): 022025.

[56] P Pradhan, O G Dahlhaug, P N Joshi. *Report on Sediment and efficiency measurement at Jhimruk hydropower plant–monsoon 2003*. Hydro Lab, Nepal, 2004.

[57] B Thapa, H Brekke. Effect of sand particle size and surface curvature in erosion of hydraulic turbine. *IAHR Symposium on Hydraulic Machinery and Systems*, Stockholm, 2004.

[58] I H Jung, Y S Kim, D H Shin, et al. Influence of spear needle eccentricity on jet quality in micro Pelton turbine for power generation. *Energy*, 2019, 175: 58-65.

[59] I C Jo, J H Park, J W Kim, et al. Jet quality characteristics according to nozzle shape of energy-recovery Pelton turbines in pressure-retarded osmosis. *Desalination and Water Treatment*, 2016, 57(51): 24626-24635.

[60] M Peron, E Parkinson, L Geppert, et al. Importance of jet quality on Pelton efficiency and cavitation. *International Conference on Hydraulic Efficiency Measurements*, Milan, Italy, 2008: 3-6.

[61] B R Cobb, K V Sharp. Impulse (Turgo and Pelton) turbine performance characteristics and their impact on pico-hydro installations. *Renewable Energy*, 2013, 50: 959-964.

[62] A K Rai, A Kumar, T Staubli. Hydro-abrasive erosion in Pelton buckets: Classification and field study. *Wear*, 2017, 392-393: 8-20.

[63] R Maldet. Pelton runner with high erosion caused by glacier sediment: Assessment and measures. *Proceedings of the15th Int. Semin. HPPs ed E Doujak (Vienna, Austria)*, 2008: 639-646.

[64] T Bovet. Contribution to the study of the phenomenon of abrasive erosion in the realm of hydraulic turbines. *Bull. Tech. Suisse Romande*, 1958, 84(3): 37-49.

[65] H J Amarendra, P Kalhan, G P Chaudhari, et al. Slurry erosion response of heat treated 13Cr-4Ni Martensitic stainless steel. *Materials Science Forum*, 2012: 500-505.

[66] G R Desale, B K Gandhi, S C Jain. Particle size effects on the slurry erosion of aluminium alloy (AA 6063). *Wear*, 2009, 266(11): 1066-1071.

[67] V Javaheria, D Portera, V T Kuokkalab. Slurry erosion of steel – Review of tests, mechanisms and materials. *Wear*, 2018: 408-409.

[68] Y Xu, Z Zhang, X W Cheng, et al. Numerical simulation of abrasive erosion in the liquid-solid two-phase rotary flow. *Journal of Beijing University of Chemical Technology (Natural Science Edition)*, 2002, 29(3): 12-16. (in Chinese)

[69] J Liu, L Lu, L Zhu. Experiment study on sediment erosion of Pelton turbine flow passage component material. *IOP Conference Series Earth and Environmental Science*, 2012, 15(3): 032055.

[70] J Liu, L Lu, L Zhu, et al. Experimental study on sediment abrasion of flow passage components of Pelton turbine. *The 19th China Hydropower equipment Symposium*, Dalian, China, 2013: 424-428. (in Chinese)

[71] R Thakur, A Kumar, S Khurana,et al. Correlation development for erosive wear rate on Pelton turbine buckets. *International Journal of Mechanical and Production Engineering Research and Development*, 2017, 7: 259-274.

[72] A K Rai, A Kumar, T Staubli. *Design and verification of a Pelton turbine rig for hydroabrasive erosion testing*. Current Research in Hydraulic Turbines (CRHT)—CRHT-VIII- 2018, 2018.

[73] IEC62364, Hydraulic machines—Guide for dealing with hydro-abrasive erosion in Kaplan, Francis and Pelton turbines. 2013.

[74] J Liu, J C Yu, L P Pan, et al. Study on performances of WC-12Co HVAF coating against cavitaion, silt erosion and abrasion. *Journal of Hydroelectric Engineering*, 2012, 31(3): 230-233+239. (in Chinese)

[75] J Liu, H Y Xu, S Tang, et al. Study on formation causes of ripple-like abrasion on hydraulic machine surfaces due to solid-liquid flow. *Journal of China Institute of Water Resources and Hydropower Research*, 2008, 2: 144-148. (in Chinese)

[76] G F Truscott. A literature survey on abrasive wear in hydraulic machinery. *Wear*, 1972, 20(1): 29-50.

[77] W Peng, X Cao, L Ma, et al. Sand erosion prediction model for two-phase flow pipe bends and its application in gas-liquid-solid multiphase flow erosion. *Powder Technology*, 2023: 118421.

[78] E Bardal. *Corrosion and corrosion protection*. Tapir, 1994.

[79] X Li, Y Feng, K E Gray. A hydro-mechanical sand erosion model for sand production simulation. *Journal of Petroleum Science and Engineering*. 2018, 166: 208-224.

[80] G L DNV. Managing sand production and erosion. Recommended Practice DNVGL-RP-O501, DNV GL Company, Oslo, Norway, 2015.

[81] D Felix, A Abgottspon, I Albayrak, et al. Hydro-abrasive erosion on coated Pelton runners: Partial calibration of the IEC model based on measurements in HPP Fieschertal. *IOP Conference Series: Earth and Environmental Science*, 2016, 49(12): 122009.

[82] H Brekke, E Bardal, T Rogne. Norwegian research work on erosion resistive coating for water turbines. *XVII IAHR Symposium*, Beijing, China, 1994: 1337-1346.

[83] M K Padhy, R P Saini. Study of silt erosion mechanism in Pelton turbine buckets. *Energy*, 2012, 39(1): 286-393.

[84] A K Rai, A Kumar, T Staubli. Forces acting on particles in a Pelton bucket and similarity considerations for erosion. *IOP Conference Series Earth and Environmental Science*, 2016, 49(12): 122002.

[85] M Toshima, T Okamura, J Sato. Basic study of coupled damage caused by silt abrasion and cavitation erosion: 2nd Report, Experiments with water channel. *Trans. Jpn. Soc. Mech. Eng. Series B*, 1991, 57(539): 2186.

[86] L I Shengcai. Cavitation enhancement of silt erosion-an envisaged micro model. *Wear*, 2006, 260(9-10): 1145-1150.

[87] GB/T, 19184-2003, Cavitation pitting evaluation in Bucket Turbine, 2003. (in Chinese)

[88] U Dorji, R Ghomashchi. Hydro turbine failure mechanisms: An overview. *Engineering Failure Analysis*, 2014, 44: 136-147.

[89] S Khurana, H S Navtej. Effect of cavitation on hydraulic turbines-A review. *International Journal of Current Engineering and Technology*, 2012, 2(1): 172-177.

[90] A Rossetti, G Pavesi, G Ardizzon, et al. Numerical analyses of cavitating flow in a pelton turbine. *Journal of Fluids Engineering, Transactions of the ASME*, 2014, 136(8): 081304.

[91] E Ayli. Cavitation in hydraulic turbines. *International Journal of Heat and Technology*, 2019, 37(1): 334-344.

[92] D Jošt, A Škerlavaj, V Pirnat, et al. Detailed analysis of flow in two Pelton turbines with efficiency and cavitation prediction. *International Journal of Fluid Machinery and Systems*, 2019, 12(4): 388-399.

[93] W T Zhou, X Q Zhou. Design of the Pelton turbine runner. *Large Electric Machine and Hydraulic Turbine*, 2008, (2): 44-53. (in Chinese)

[94] B Thapa, P Chaudhary, O G Dahlhaug, et al. Study of combined effect of sand erosion and cavitation in hydraulic turbines. *International Conference on Small Hydropower-Hydro Sri Lanka*, 2007: 24.

[95] N M He. Causes and prevention of cavitation and erosion of large bucket runner in Tianwan River. *Mechanical & Electrical Technique of Hydropower Station*, 2013, 36(6): 8-10. (in Chinese)

[96] S Chitrakar, B W Solemslie, H P Neopane, et al. Review on numerical techniques applied in impulse hydro turbines. *Renewable Energy*, 2020, 159: 843-859.

[97] S Schuster, F K Benra, H J Dohmen. *Numerical simulation of a micro Pelton turbine working in the two-phase flow regime*. American Society of Mechanical Engineers, 24th Symposium on Fluid Machinery, 2012.

[98] J R Rygg. *CFD analysis of a Pelton turbine in openFOAM*. Trondheim: Norwegian University of Science and Technology, 2013.

[99] D Benzon, A Židonis, A Panagiotopoulos, et al. Numerical investigation of the spear valve configuration on the performance of Pelton and Turgo turbine injectors and runners. *Journal of Fluids Engineering*, 2015,137(11):111201.

[100] C Vessaz, E Jahanbakhsh, F Avellan. Flow simulation of jet deviation by rotating Pelton buckets using finite volume particle method. *Journal of Fluids Engineering*, 2015, 137(7): 074501.

[101] A Perrig. *Hydrodynamics of the free surface flow in Pelton turbine buckets*. Lausanne: EPFL, 2007.

[102] J C Marongiu, F Leboeuf, J Caro. Free surface flows simulations in Pelton turbines using an hybrid SPH-ALE method. *Journal of Hydraulic Research*, 48, 2010: 40-49.

[103] K Furnes. *Flow in Pelton turbines*. Trondheim: Norwegian University of Science and Technology, 2013.

[104] A Židonis, A Panagiotopoulos, G A Aggidis, et al. Parametric optimisation of two Pelton turbine runner designs using CFD. *Journal of Hydrodynamics*, 2015, 27(3): 403-412.

[105] Y Nakanishi, T Fujii, S Kawaguchi. Numerical and experimental investigations of the flow in a stationary Pelton bucket. *Journal of Fluid Science & Technology*, 2009, 4(3): 490-499.

[106] O G Dahlhaug, T Nielsen. Efficiency loss in Pelton buckets due to sediment erosion. *Proceedings of the 23rd IAHR Symposium on Hydraulic Machinery and Systems*, 2006: 2-7.

[107] J B Mclaughlin. Numerical computation of particle-turbulence interaction. *International Journal of Multiphase Flow*, 1994, 20(supp-S1): 211-232.

[108] W Su. *A study of solid-liquid two phase flow on inner buckets of Pelton turbines*. Chengdu: Xihua University, 2015. (in Chinese)

[109] Y Cao, W W Song, J Fu, et al. Erosion of buckets of Pelton turbine with sediment. *Water Power*, 2014, 40(7): 75-85. (in Chinese)

[110] S Wei, W W Song, F Jie, et al. A study of silt erosion on inner buckets of Pelton turbines. *Applied Mechanics and Materials*, 2015: 716-717.

[111]   B Suyesh, V Parag, D Keshav, et al. Novel trends in modelling techniques of Pelton turbine bucket for increased renewable energy production. *Renewable and Sustainable Energy Reviews*, 2019, 112: 87-101.

[112]   S Leguizamón, S Alimirzazadeh, E Jahanbakhsh, et al. Multiscale simulation of erosive wear in a prototype-scale Pelton runner. *Renewable Energy*, 2020, 151: 204-215.

[113]   M Kumar, R P Saini. CFD analysis of silt erosion in Pelton turnine. *International Conference on Hydropower for Sustainable Development*, Dehradun, 2015: 218-227.

[114]   A K Rai, A Kumar. Sediment monitoring for hydro-abrasive erosion: A field study from Himalayas, India. *International Journal of Fluid Machinery & Systems*, 2017, 10(2): 146-153.

[115]   S Leguizamón, E Jahanbakhsh, A Maertens, et al. A multiscale model for sediment impact erosion simulation using the finite volume particle method. *Wear*, 2017, 392: 202-212.

[116]   S Leguizamón, E Jahanbakhsh, S Alimirzazadeh, et al. Multiscale simulation of the hydroabrasive erosion of a Pelton bucket: Bridging scales to improve the accuracy. *International Journal of Turbomachinery, Propulsion and Power*, 2019, 4(2): 9.

[117]   S Leguizamón, E Jahanbakhsh, A Maertens, et al. Simulation of the hydroabrasive erosion of a bucket: A multiscale model with projective integration to circumvent the spatio-temporal scale separation. *IOP Conference Series: Earth and Environmental Science*, IOP Publishing, 2019, 240(7): 072014.

[118]   S Leguizamón, E Jahanbakhsh, S Alimirzazadeh, et al. FVPM numerical simulation of the effect of particle shape and elasticity on impact erosion. *Wear*, 2019, 430-431:108-119.

[119]   C J Zeng, Y X Xiao, J Zhang, et al. Numerical analysis of pelton turbine needle erosion characteristics. *Journal of Drainage and Irrigation Machinery Engineering*, 2015, 33(5): 407-411. (in Chinese)

[120]   C J Zeng, Y X Xiao, W Zhu, et al. Pelton turbine Needle erosion prediction based on 3D three-phase flow simulation. *IOP Conference Series: Earth and Environmental Science*, 2014, 22(5): 052019.

[121]   G V Messa, S Mandelli, S Malavasi. Hydro-abrasive erosion in Pelton turbine injectors: A numerical study. *Renewable Energy*, 2019, 130: 474-488.

[122]   B Guo, Y Xiao, A K Rai, et al. Sediment-laden flow and erosion modeling in a Pelton turbine injector. *Renewable Energy*, 2020, 162: 30-42.

[123]   X Ge, J Sun, Y Zhou, et al. Experimental and numerical studies on opening and velocity influence on sediment erosion of Pelton turbine buckets. *Renewable Energy*, 2021, 173: 1040-1056.

[124]   B Guo, Y Xiao, A K Rai, et al. Analysis of the air-water-sediment flow behavior in Pelton buckets using a Eulerian-Lagrangian approach. *Energy*, 2021, 218: 119522.

[125]   B Guo, Y Li, Y Xiao, et al. Numerical analysis of sand erosion for a pelton turbine injector at high concentration. *IOP Conference Series: Earth and Environmental Science*. IOP Publishing, 2021, 627(1): 012022.

[126]   D Jošt, A Škerlavaj, V Pirnat, et al. Numerical prediction of efficiency and cavitation for a Pelton turbine. *IOP Conference Series: Earth and Environmental Science*, 2019, 240(6): 062033.

[127]   Y Cao, W W Song, Q Huang. A study of solid-liquid two phase flow on inner buckets of Pelton turbines. *Science and Technology Innovation Herald*, 2014, 28: 65-66. (in Chinese)

[128]   G Nath, S G Kumar. Studies on slurry erosion of hard protective coatings on 13-4 martensitic stainless steel for hydro turbine blades. *MED*, 2017.

[129]   R E Vieira, A Mansouri, B S Mclaury. Experimental and computational study of erosion in elbows due to sand particles in air flow. *Powder Technology*, 2016, 288: 339-353.

[130]   P J Roache. Quantification of uncertainty in computational fluid dynamics. *Ann. Rev. Fluid Mech.*, 1997, 29(1): 123-160.

[131]   M Choi, Y J Jung, Y Shin. Unsteady flow simulations of Pelton turbine at different rotational speeds. *Advances in Mechanical Engineering*, 2015, 7(11): 168781401561653.

[132]   F G Stamatelos, J S Anagnostopoulos, D E Papantonis. Performance measurements on a Pelton turbine model. *Proceedings of the Institution of Mechanical Engineers, Part A: Journal of Power & Energy*, 2011, 225(3): 351-362.

[133]   Y Xiao, Z Wang, Z Jin, et al. Numerical and experimental analysis of the hydraulic performance of a prototype Pelton turbine. *Proceedings of the Institution of Mechanical Engineers, Part A: Journal of Power & Energy*, 2014, 228(1): 46-55.

[134]   R E Vieira, A Mansouri, S Brenton, et al. Experimental and computational study of erosion in elbows due to sand particles in air flow. *Powder Technology*, 2016, 288: 339-353.

[135]   F Muggli, Z Zhang, C Schärer, et al. Numerical and experimental analysis of pelton turbine flow, Part 2: The free surface jet flow. *The 20th IAHR Symposium on Hydraulic Machinery and Systems*, Charlotte, 2000: 6-9.

[136]   M Hana. Improvements of a graphical method for calculation of flow on a Pelton bucket. *Hydraulic Machinery and Cavitation*, 1996: 111-119.

[137]   Y X Xiao, F Q Han, J L Zhou, et al. Numerical prediction of dynamic performance of Pelton turbine. *Journal of Hydrodynamics*, 2007, 19(3): 356-364.

[138]   P K Koukouvinis, J S Anagnostopoulos, D E Papantonis. Numerical computation of the performance curve of a pelton turbine using the smoothed particle hydrodynamics method. *The 7th GRACM Congress hosts the 1st ECCOMAS PhD Olympiad 2011*, 2011: 1-10.

[139]   K Kan, Y Zheng, H Chen, et al. Numerical simulation of transient flow in a shaft extension tubular pump unit during runaway process caused by power failure. *Renewable Energy*, 2020, 154: 1153-1164.

[140]   K Kan, H Chen, Y Zheng, et al. Transient characteristics during power-off process in a shaft extension tubular pump by using a suitable numerical model. *Renewable Energy*, 2020, 164: 109-121.

[141]   Y Zhang, J Zhang, X Lin, et al. Experimental investigation into downstream field of a horizontal axis tidal stream turbine supported by a mono pile. *Applied Ocean Research*, 2020, 101:102257.

[142]   Y Zhang, E Fernandez-Rodriguez, J Zheng, et al. A review on numerical development of tidal stream turbine performance and wake prediction. *IEEE Access*, 2020, 8: 79325-79337.

[143]   J Veselý, M Varner. A case study of upgrading of 62.5 MW Pelton turbine. *Proceedings of the International Conference, IAHR*, 2001. http://www.davar.cz/corfat/pdf/A_case_study.pdf.

[144]   D Adanta, N S Puta, H Vohra. Cutout types analysis on pico hydro Pelton turbine. *International Journal on Advanced Science, Engineering and Information Technology*, 2018, 8(5): 2024-2030.

[145]   J You, X Lai, W Zhou, et al. 3D CFD simulation of the runaway process of a Pelton turbine. *Proceedings of the Institution of Mechanical Engineers, Part A: Journal of Power and Energy*, 2016, 230(2): 234-244.

[146]   Y Q Jiang. *Flow-induced vibration analysis Pelton turbine*. Wuhan: Wuhan University, 2017. (in Chinese)

[147]   X Q Zhou, W T Zhou, G J Yin, et al. Numerical test rig for Pelton turbine(1). *The 19th China Hydropower Equipment Symposium*, Dalian, China, 2013: 436-441. (in Chinese)

[148]   X Q Zhou, W T Zhou, G J Yin, et al. Numerical test rig for Pelton turbine (2). *The 19th China Hydropower Equipment Symposium*, Dalian, China, 2013: 442-448. (in Chinese)

[149]   P E Smirnov, F R Menter. Sensitization of the SST turbulence model to rotation and curvature by applying the Spalart-Shur correction term. *Journal of Turbomachinery*, 2009, 131(4): 041010.

[150]   V Sammartano, G Morreale, M Sinagra, et al, Numerical and experimental investigation of a cross-flow water turbine. *Journal of Hydraulic Research*, 2016, 54(3): 321-331.

[151]   S Petley, A Židonis, A Panagiotopoulos, et al. Out with the old, in with the New: Pelton hydro turbine performance influence utilizing three different injector geometries. *Journal of Fluids Engineering*, 2018, 141(8): 081103.

[152]   R F L de Cerqueira, R M Perissinotto, W M Verde, et al. Development and assessment of a particle tracking velocimetry (PTV) measurement technique for the experimental investigation of oil drops behaviour in dispersed oil–water two-phase flow within a centrifugal pump impeller. *International Journal of Multiphase Flow*, 2023, 159: 104302.

[153]   Y I Oka, T Yoshida. Practical estimation of erosion damage caused by solid particle impact. Part 2: Mechanical properties of materials directly associated with erosion damage. *Wear*, 2005, 259(1-6): 102-109.

[154]   Y I Oka, K Okamura, T Yoshida. Practical estimation of erosion damage caused by solid particle impact: Part 1: Effects of impact parameters on a predictive equation. *Wear*, 2005, 259(1-6): 95-101.

[155]   K Haugen, O Kvernvold, A Ronold, et al. Sand erosion of wear-resistant materials: Erosion in choke valves. *Wear*, 1995, (s 186-187): 179-188.

Ge *et al. Chinese Journal of Mechanical Engineering*　　(2023) 36:64

Page 26 of 27

[156] G Grant, W Tabakoff. Erosion Prediction in turbomachinery resulting from environmental solid particles. *Journal of Aircraft*, 2012, 12(5): 471-478.

[157] J H Neilson, A Gilchrist. Erosion by a stream of solid particles. *Wear*, 1968, 11(2): 111-122.

[158] I Finnie. Erosion of surface by solid particles. *Wear*, 1960, 3(2): 87-103.

[159] J H Su, Z W Guo. The applicability of erosion models based on erosion equations. *China Rural Water and Hydropower*, 2019, 4: 104-109. (in Chinese)

[160] G V Messa, S Malavasi. The effect of sub-models and parameterizations in the simulation of abrasive jet impingement tests. *Wear*, 2017, 370: 59-72.

[161] H Zhu, J Zhu, R Rutter, et al. Sand erosion model prediction, selection and comparison for electrical submersible pump (ESP) using CFD method. *Fluids Engineering Division Summer Meeting*, American Society of Mechanical Engineers, 2018: V003T17A003.

[162] M Sick, H Keck, E Parkinson, et al. New challenges in pelton research. *Hydro Conference*, Bern, Switzerland, 2000. http://www.flow3d.com/pdfs/tp/general/new-challenges-in-pelton-research-3-01.pdf.

[163] C J Zeng, Y X Xiao, W Zhu, et al. Numerical simulation of cavitation flow characteristic on Pelton turbine bucket surface. *IOP Conference Series: Materials Science and Engineering*, 2015, 72(4): 042043.

[164] Y Ding. Selection of turbine for CLH Hydropower Station. *Small Hydro Power*, 2020, (3) 41-43. (in Chinese)

[165] J Y Xing, Z D Xie. Study on sand reduction and flushing system of CCS hydropower station with large flow and high sediment concentration. *Yellow River*, 2019, 41(12): 23-25+34. (in Chinese)

[166] B P Shrestha, B Gautam, T R Bajracharya. Computational analysis of Pelton bucket tip erosion using digital image processing. *Electronic Imaging and Multimedia Technology V, SPIE*, 2007: 68333C.

[167] S H Gu, R Q Jia, Y Y Zhang, et al. Abrasion and control of turbine. *Design of Water Resources & Hydroelectric Engineering*, 2011, 30(1): 39-43. (in Chinese)

[168] B S Thapa, B Thapa, O G Dahlhaug. Current research in hydraulic turbines for handling sediments. *Energy*, 2012, 47(1): 62-69.

[169] Z Y Mei, Y L Wu. Review of research on abrasion and cavitation of silt-laden flow through hydraulic turbine runner in China. *Proc. of the 19th IAHR, Section of Hydraulic Machinery and Cavitation*, Valencia, 1996: 641-650.

[170] H P Neopane, M Cervantes. Sediment erosion in hydraulic turbines. *Global Journal of Research Engineering*, 2011, 11(6): 17-26.

[171] N Faletti. Erosion and corrosion of hydraulic turbines. *L'energia elettrica*, 1934, 11: 277.

[172] Z Wang, N Long, J Zhu. Review on material resistant to cavitation erosion and its application. *Dev. Appl. Mater.*, 2001, 6: 34-38.

[173] E Mònica, E Eduard, V Carme, et al. Advanced condition monitoring of Pelton turbines. *Measurement*, 2018, 119: 46-55.

[174] G An. Design of large Pelton turbine for Gongger Hydropower Station. *Small Hydro Power*, 2018, (5): 45-47. (in Chinese)

[175] W S Ebhota. *Novel domestic design and manufacturing of Pelton Turbine bucket: a key to manage and enhance Sub-Saharan Africa's hydro energy potential*. Pietermaritzburg: University of Kwazulu-Natal, 2017.

[176] Z Gao, X Feng, S Liu, et al. Key technologies of large and medium-sized Pelton-Turbine. *Large Electric Machine and Hydraulic Turbine*, 2021, (3): 63-68. (in Chinese)

[177] T He, Z Liu, J Wang, et al. Strength calculation and hydrostatic test of the distributor of Pelton turbine at the level of kilometer. *Large Electric Machine and Hydraulic Turbine*, 2020, (2): 81-86. (in Chinese)

[178] Z Zheng, Z Li, X Wei, et al. Structure constant G and streamline similarity method for flow distributions at the low pressure sides of the pump and the turbine impellers. *Large Electric Machine and Hydraulic Turbine*, 2018, (1): 1-9. (in Chinese)

[179] G F Yue, Y P Li, D X Chen. Modification of hydraulic turbine under abrasion and erosion on Sediment-laden River. *Water Power*, 2010, 36(5): 56-58. (in Chinese)

[180] L Zhang, X M Chen, Y M Wu, et al. Technological advances in coatings for abrasion-cavitation erosion protection of hydraulic turbine flowparts. *Materials Review*, 2017, 31(17): 75-83. (in Chinese)

[181] A Karimi, C Verdon, J L Martin, et al. Slurry erosion behaviour of thermally sprayed WC-M coatings. *Wear*, 1995, 186: 480-486.

[182] J H Gummer. Combating silt erosion in hydraulic turbines-Some of the most attractive hydro sites are plagued by silt. *Hydro Review Worldwide*, 2009, 17(1): 28.

[183] L Thakur, N Arora. A study of processing and slurry erosion behaviour of multi-walled carbon nanotubes modified HVOF sprayed nano-WC-10Co-4Cr coating. *Surface and Coatings Technology*, 2017, 309: 860-871.

[184] J F Santa, J A Blanco, J E Giraldo, et al. Cavitation erosion of martensitic and austenitic stainless steel welded coatings. *Wear*, 2011, 271(9-10): 1445-1453.

[185] L R Wang, Y M Wu, X M Chen, et al. Study on mechanical property and fracture mechanism of ceramic particle-reinforced epoxy composite coating. *Electroplating & Finishing*, 2015, 34(22): 1288.

[186] R Z Zhang, W Lu, D K Yan, et al. Abrasion resistance analysis of spray polyurethane elastic coating on turbine blades. *Surface Technology*, 2014, 43(01): 11-15. (in Chinese)

[187] D A Karandikar. HVOF coatings to combat hydro abrasive erosion. *Int. Conf. Hydropower Sustain. Dev.*, Dehradun, India, 2015: 171-179.

[188] A Kafle, P L Shrestha, S Chitrakar, et al. A review on casting technology with the prospects on its application for hydro turbines. *Journal of Physics: Conference Series*, IOP Publishing, 2020, 1608(1): 012015.

[189] E E Mon, C C Khaing, A Zaw Lynn. Design, construction and performance testing of 1 kW Pelton turbine for pico hydro power plant. *Int. J. Sci. Eng. Appl.*, 2019, 8(07): 192-196.

[190] T Li, W Chen, C Chen. Rough machining method for blisk plunge milling. *Computer Integrated Manufacturing Systems*, 2010, (8): 1696-1701.

[191] B Wang, X L Liu, C X Yue, et al. Study on NC machining technology for integral impeller of Pelton turbine. *Advanced Materials Research. Trans Tech Publications Ltd.*, 2010, 102: 861-865.

[192] G C Chaudhari, D S A Channiwala, S P Shah. Comparative assessment of the developed stress in both traditional and hooped Pelton runners. *Tenth International Congress of Fluid Dynamics*, Ain Soukhna, Red Sea, Egypt, 2010. https://www.researchgate.net/publication/303551506.

[193] T Weiss, Y T Ma. Modern manufacturing technology of impact runners. *Express Water Resources & Hydropower Information*, 2010, 31(4): 27-28+41. (in Chinese)

[194] B L Wang, X L Liu, J S Liu, et al. Structural optimization and manufacturing for region of high stress of Pelton turbine. *Journal of Mechanical Engineering*, 2015, 51(21) : 148-155. (in Chinese)

[195] A Panthee, B Thapa, H P Neopane. Quality control in welding repair of Pelton runner. *Renewable Energy*, 2015, 79: 96-102.

[196] L Yeshi, S Choki. Quantifiable crack detection in newly installed Pelton turbine. *DEStech Transactions on Computer Science and Engineering*, 2016.

[197] D Felix, I Albayrak, R M Boes, et al. Dealing with Pelton turbine erosion based on systematic monitoring. *Hydropower and Dams*, 2018, 25(5): 84-92.

[198] A Abgottspon, T Staubli, D Felix, et al. Hydro-abrasive erosion of Pelton buckets and suspended sediment monitoring. *Proceedings of the Hydro Vision International*, Denver, USA, 2013. https://www.researchgate.net/publication/291339891.

[199] L Selak, P Butala, A Sluga. Condition monitoring and fault diagnostics for hydropower plants. *Computers in Industry*, 2014, 65(6): 924-936.

[200] I F Pachón, J Loboguerrero, J A Medina. Development of a test rig to evaluate abrasive wear on Pelton turbine nozzles, A case study of Chivor hydropower. *Wear*, 2017, 372: 208-215.

[201] P Bachmann. Experimental flow studies on a 1-jet model Pelton turbine. *Proceedings of 15th IAHR Symposium on Modern Technology in Hydraulic Energy Production*, Sept. 11–14, Belgrade, Yugoslavia, Faculty of Mechanical Engineering, Belgrade, 1990: 1-13.

[202] G Chaudhari, S Channiwala, S Shah, et al. Flow visualization study of jet and bucket interactions in traditional and hooped Pelton runner. *Fluids Engineering Division Summer Meeting*, American Society of Mechanical Engineers, 2019: V03BT03A069.

[203] G Neubacher, H Humm, T Staubli. Poor jet quality as a cause of noise in Pelton turbines. *Ninth International Hydropower Symposium*, 1996. https://www.researchgate.net/publication/290430461.

[204] M E Gass. Mechanical rehabilitation: Lessons learned at Moccasin Powerhouse. *Hydro Review*, 2003, 22(1): 10-13.

[205] A K Rai, A Kumar, T Hies, et al. Field application of a multi-frequency acoustic instrument to monitor sediment for silt erosion study in Pelton

Ge *et al. Chinese Journal of Mechanical Engineering*   *(2023) 36:64*

Page 27 of 27

turbine in Himalayan region, India. *IOP Conference Series Earth and Environmental Science*, 2016, 49(12): 122004.

[206] A K Rai, A Kumar. Analyzing hydro abrasive erosion in Kaplan turbine: a case study from India. *Journal of Hydrodynamics*, 2016, 28(5): 863-872.

[207] R Boes. Real-time monitoring of suspended sediment concentration and particle size distribution in the headwater way of a high-head hydropower plant. *Water Engineering for Sustainable Environment: 33rd IAHR Congress*, 2009: 4037-4044.

[208] A K Rai, A Kumar. Continuous measurement of suspended sediment concentration: Technological advancement and future outlook. *Measurement*, 2015, 76: 209-227.

[209] D Felix, I Albayrak, R M Boes. Continuous measurement of suspended sediment concentration: Discussion of four techniques. *Measurement*, 2016, 89: 44-47.

[210] H P Neopane, S Sujakhu. Particle size distribution and mineral analysis of Sediments in Nepalese hydropower plant: A case study of Jhimruk hydropower plant. *Kathmandu University Journal of Science, Engineering and Technology*, 2013, 9(1): 29-36.

[211] V Mano, J Nemery, P Belleudy, et al. Assessment of suspended sediment transport in four alpine watersheds (France): influence of the climatic regime. *Hydrological Processes: An International Journal*, 2009, 23(5): 777-792.

[212] O Navratil, M Esteves, C Legout, et al. Global uncertainty analysis of suspended sediment monitoring using turbidimeter in a small mountainous river catchment. *Journal of Hydrology*, 2011, 398(3-4): 246-259.

[213] Y S Hsu, J F Cai. Densimetric monitoring technique for suspended-sediment concentrations. *Journal of Hydraulic Engineering*, 2010, 136(1): 67-73.

[214] D Felix, I Albayrak, R M Boes. In-situ investigation on real-time suspended sediment measurement techniques: Turbidimetry, acoustic attenuation, laser diffraction (LISST) and vibrating tube densimetry. *International Journal of Sediment Research*, 2018, 33(1): 3-17.

[215] D Felix, I Albayrak, A Abgottspon, et al. Suspended sediment measurements and calculation of the particle load at HPP Fieschertal. *IOP Conference Series: Earth and Environmental Science*, 2016, 49(12): 122007.

[216] M Haimann, M Liedermann, L Petra, et al. An integrated suspended sediment transport monitoring and analysis concept. *International Journal of Sediment Research*, 2014, 29(2): 135-148.

[217] G W Lin, H Chen, D N Petley, et al. Impact of rainstorm-triggered landslides on high turbidity in a mountain reservoir. *Engineering Geology*, 2011, 117(1-2): 97-103.

[218] D Felix, I Albayrak, A Abgottspon, et al. Real-time measurements of suspended sediment concentration and particle size using five techniques. *IOP Conference Series: Earth and Environmental Science*, IOP Publishing, 2016, 49(12): 122006.

[219] M Egusquiza, E Egusquiza, D Valentin, et al. Failure investigation of a Pelton turbine runner. *Engineering Failure Analysis*, 2017, 81: 234-244.

[220] M Egusquiza, C Valero, A Presas, et al. Experimental investigation on the dynamic response of Pelton runners. *IOP Conference Series: Earth and Environmental Science*, 2019, 240(2): 022062.

[221] A Åsnes, A Willersrud, F Kretz, et al. Predictive maintenance and life cycle estimation for hydro power plants with real-time analytics. 2018. https://www.researchgate.net/publication/328879561.

[222] A Ø Åsnes. *Condition monitoring of hydroelectric power plants*. Trondheim: NTNU, 2018.